

Rift and plume: a discussion on active and passive rifting mechanisms in the Afro-Arabian rift based on synthesis of geophysical data

Ran Issachar^{1,2}, Peter Haas^{1,3}, Nico Augustin³ and Jörg Ebbing¹

¹Institute for Geosciences, Kiel University, Geophysics, Kiel, Deutschland, ²Geological Survey of Israel, Jerusalem, Israel,

³GEOMAR Helmholtz Centre for Ocean Research, [Dynamics of the Ocean Floor](#), Kiel, Deutschland

Correspondence to: Ran Issachar (ranis@gsi.gov.il)

Abstract

The causal relationship between the activity of mantle plumes and continental break-up is still elusive. The Afro-Arabian rift system offers an opportunity to examine these ~~relationships~~ [relationship](#), in which an ongoing continental break-up intersects a large Cenozoic ~~plume-related~~ [plume-related](#) flood basalt series. In the Afar region, the Gulf of Aden, the Red ~~Sea~~ and the Main Ethiopian Rift form an R-R-R triple junction, ~~separating and separate~~ the Ethiopian and Yemen Traps by ~600 km. We provide an up-to-date synthesis of the available geophysical and geological data from this region. We map the rift architecture in the intersection region of the rifts and review the spatio-temporal constraints in ~~developing the development of~~ the different features of the plume-rift system.

We infer two spatial constraints in the development of the rifts: (1) the connection of the Main Ethiopian Rift to the Gulf of Aden and ~~to~~ the Red Sea by its northeastward propagation; (2) the abandonment of an early tectonic connection between the Red Sea and the Gulf of Aden. Additionally, chronological evidence suggests that regional uplift and flood basalt eruptions sufficiently preceded rifting. By this, we infer a progressive development in which the onset of the triple junction marks a tectonic reorganization and was the last feature to develop, after all rift arms were thoroughly developed. We argue that the classical active and passive rifting mechanisms cannot simply explain the progressive development of the Afro-Arabian rift and propose a scenario of plume-induced plate rotation that includes an interaction between active and passive mechanisms. In this scenario, the arrival of the Afar plume provided a ~~push force~~ [push-force](#) that promoted the rotation of Arabia around a nearby pole, enabling ~~the~~ rifting and, ultimately, the break-up of Arabia from Africa.

28

Short summary:

We explore the causal relationship between the arrival of the Afar plume and the initiation of the Afro-Arabian rift. We mapped the rift architecture in the triple junction region from geophysical data and reviewed the available geological temporal evidence. We infer a progressive development of the plume-rift system and suggest an interaction between active and passive mechanisms in which the plume provided a push-force that changed the kinematics of the associated plates.

35 1. Introduction

36 The causal dependency between the eruption of flood basalts and continental break-up is still unclear,
37 although a close occurrence between these two phenomena has been recognized for a long time.
38 Continental flood basalts, often referred to as traps, form large igneous provinces covering huge
39 continental areas (Bryan and Ferrari, 2013; Ernst, 2014). ~~Continental flood basalts~~ They are often
40 associated with extensive volcanism during short time intervals, ~~which are~~ brought to the surface by deep-
41 seated mantle plumes (Richards et al., 1989; White and McKenzie, 1995; Koppers et al., 2021), ~~although~~
42 ~~other mechanisms were also suggested~~ (e.g., Anderson, 1994, 2005). ~~Observations indicate~~ There is
43 ~~evidence for~~ a close temporal and spatial occurrence between the eruption of flood basalts and
44 continental break-up. In particular, when reconstructed back to their original plate tectonic configuration,
45 ~~an~~ R-R-R triple junction is ~~typically~~ found within the flood ~~basalt~~basalts areas (Morgan, 1971; Burke and
46 Dewey, 1973; Buitter and Torsvik, 2014). Using the geological record to examine the mutual dependency
47 of these processes is challenging. It requires high-precision constraints regarding the temporal and spatial
48 development of the different volcanic and tectonic features, often obscured by the long geological history.

49 The Afar region in the central parts of the Afro-Arabian rift system is recognized as a key locality to examine
50 models of plume-rift association, offering a young and active case study in which plume, regional uplift, R-
51 R-R triple junction, break-up, and oceanic spreading co-exist and are superimposed (Fig. 1). Plume-rift
52 association is mainly explained by either ‘active’ (e.g., Sengör and Burke, 1978) or ‘passive’ (e.g., White
53 and McKenzie, 1989) views, with no interaction between those modes. ~~However,~~ ~~although~~ some evidence
54 ~~suggests~~ ~~suggest~~ a more complex effect of plumes on the regional plate kinematics (e.g., Cande and
55 Stegman, 2011). Despite the contrary implications of the ‘active’ and ‘passive’ views, the Afar case study
56 was used as a prime example to support both, and some authors argued that both processes are required
57 to explain the observations (Burke and Dewey, 1973; White and McKenzie, 1989; Courtillot et al., 1999).
58 The discrepancy can be primarily attributed to a lack of accurate geological and geophysical evidence,
59 leading to contrary interpretations.

60 The purpose of this paper is to utilize a synthesis of the available geological and geophysical data from the
61 Afar region and to use it for geodynamic implications in the study area. We first review the evidence
62 regarding the temporal association of the volcanic and rift components of the system. This review is
63 essential because large amounts of new data were collected in recent years, enabling a re-examination of
64 the relationships between the plume and the rifting. We further provide an analysis and interpretation of
65 modern geophysical datasets, including topography, bathymetry, gravity, magnetic anomalies,
66 earthquakes, and volcano distribution. Using these datasets, we map the architecture of the rift margins
67 and axes and infer spatial constraints in ~~developing~~ ~~the development of~~ the rift segments. Finally, we
68 discuss the results in the light of recent models and ~~from~~ other case studies in the world, aiming to shed
69 light on the causal relationship between mantle plumes and tectonic processes in the crust.

70 2. Active and passive mechanisms for plume-rift association

71 The existence of deep mantle convection and its interaction with the Earth’s ~~crust~~ ~~lithosphere~~ was already
72 pointed out by Wilson (1963), and a close occurrence to continental break-up was soon noticed by the
73 abundance of hotspots near many rift junctions (Morgan, 1971) and flood basalts volcanism along passive
74 margins (Richards et al., 1989). ~~This led~~ ~~Although~~ Morgan (1971) ~~to~~ ~~speculated~~ ~~d~~ that deep mantle

75 convection has a significant role in accelerating the overlying tectonic plates. ~~Nevertheless~~, it was later
76 realized that slab-pull provides the main driving force for plate motion (Forsyth and Uyeda, 1975).
77 ~~Furthermore, plumes are thought to have a major role in plate tectonics, triggering rifting by weakening~~
78 ~~the upper lithosphere.~~ In their landmark paper, Burke and Dewey (1973) presented 45 case studies of rift
79 junctions associated with hot spots. They proposed a model in which plume-associated uplift and
80 volcanism precede and generate the rift arms, ~~which~~ initiated from a triple junction within the plume
81 region. Afar was used as a first and prime example, highlighting its importance as a young and active case
82 study; however, they already noted its complexity (Burke and Dewey, 1973).

83 Following these insights, 'active' rifting models were developed to explain plume-rift associations (e.g.,
84 Keen, 1985; Moretti and Froidevaux, 1986; Campbell and Griffiths, 1990; Hill, 1991; White and McKenzie,
85 1995). These models generally propose that rifting can result from a combination of processes derived
86 ~~from~~by the actively rising head ~~of an anomalously of anomalously~~ hot mantle. These include impinging and
87 eroding the base of the lithosphere, which ~~prompts~~~~prompt~~ uplift and decompression melting, which in
88 turn introduces internal extensional forces and ultimately leads to break-up. Accordingly, in this view,
89 regional uplift and volcanism are expected to precede rifting, which would initiate from a triple junction
90 above the mantle plume head (Fig. 2a).

91 Later contributions challenged the active view, arguing that a 'passive' asthenospheric upwelling can also
92 resolve the occurrence of flood basalt near rifts (firstly introduced by White and McKenzie, 1989). In this
93 view, rifting is initiated by the remote stresses, usually along former sutures and weak zones, regardless
94 of underlying plumes. The production of massive volcanism is allowed when the thinned and stretched
95 lithosphere is underlain by a thermal anomaly in the mantle. The volcanism is generated by decompression
96 melting of the hot asthenospheric mantle, passively rising. As plumes form large areas of higher
97 temperatures in the mantle, massive volcanism is found on ~~earth's~~ Earth's crust close to rifts. Accordingly,
98 in this view, subsidence is a precondition required for magmatism, and there is no particular reason for a
99 triple junction to form within the flood basalts region (Fig. 2b).

100 Although active and passive views have been discussed in the last 50 years, the role of plumes in initiating
101 rifting is still unclear and much debated. Even for well-studied and prime examples of plume-rift
102 association as the Siberian, Parana-Etendeka, Deccan, and Greenland traps, there is no agreement on
103 whether active processes initiated rifting (Geoffroy, 2005; Ivanov et al., 2015; Frizon De Lamotte et al.,
104 2015; Fromm et al., 2015; Mitra et al., 2017). Some authors emphasize the significance of preexisting
105 lithosphere weaknesses along structural inheritance and former sutures (Buiter and Torsvik, 2014; Will
106 and Frimmel, 2018), while others show the potential of plumes to thermally and chemically erode the base
107 of the lithosphere in the weakening process allowing rifting (Sobolev et al., 2011). Additionally, some
108 models demonstrate that mixed active-passive scenarios can better explain observation (Koptev et al.,
109 2018), and even that both mechanisms are needed to explain temporal variations in rifts (Huismans et al.,
110 2001).

111 In addition to the dichotomic views, some evidence ~~implies~~~~simply~~ more complex relationships between
112 plumes ~~—~~and the kinematics of the associated plates (van Hinsbergen et al., 2011; Cande and Stegman,
113 2011; Chatterjee et al., 2013; Pusok and Stegman, 2020). These studies discuss the role of plumes in
114 changing the relative motions of the overlying plates and suggest that lateral forces, induced by the arrival
115 of the plume head, can add up to the remote stresses, change the plate kinematics and even trigger the
116 formation of new plate boundaries (van Hinsbergen et al., 2021) (Fig. 2c). Thus, in this view the plume is
117 changing the remote stress field, which in-turn allows rifting.

118 3. Geological setting

119 The Afro-Arabian rift system ~~extendsis~~ extending from Turkey to Mozambique (McConnell and Baker,
120 1970) and is the current episode of the Phanerozoic break-up of the East African continental plate
121 (Bosworth, 2015). It contains ~~the~~ rifting in the Gulf of Aden, in the Red Sea, and in East Africa. In the center
122 of that system, the Ethiopian northwestern and southeastern plateaus represent an elevated topography
123 with a highest peak of 4,620 m (Ras Dashan) and an average elevation of 2000 m above sea level. This area
124 is part of the so-called African Superswell, a wide region of anomalously high topography comprising East
125 Africa (Lithgow-Bertelloni and Silver, 1998; Corti, 2009). In western Yemen, the Sarawat Mountains are the
126 highest peaks in the Arabian Peninsula, reaching more than 3,000 m, at only 100 km from the shoreline of
127 the Red Sea. The mountains show a typical stair morphology with steep slopes at the western and southern
128 sides, while the eastern side ~~of the mountains~~ slopes downward more gently.

129 The Gulf of Aden is the most developed rift segment in the Afro-Arabian rift, with a mature and fully
130 developed oceanic spreading center connected to the mid-ocean ridge in the Indian Ocean. Six pairs of
131 magnetic ~~stripes-anomalies associated with seafloor spreading~~ are recognized along the Gulf of Aden ~~ridge~~
132 (Fournier et al., 2010) (Fig. 3). Oblique rifting and ~~high-angle~~ high-angle structural inheritance along the
133 Gulf of Aden resulted in multiple ridge segments and fracture zones (i.e., transform faults; Leroy et al.,
134 2013; Autin et al., 2013; Bellahsen et al., 2013; Duclaux et al., 2020).

135 At the northern parts, rifting in the Red Sea is connected by the Dead Sea Fault to the Eurasian collision
136 zone along the Taurus-Zagros Mountains. The Red Sea is ~~currently~~ experiencing the last stages of break-
137 up and early stages of oceanic accretion. An oceanic spreading center with three pairs of ridge parallel
138 magnetic ~~stripes-anomalies~~ is developed in the southern parts of the Red Sea (Schettino et al., 2016) (Fig.
139 3). However, oceanic crust is probably flooring most of the basin (Augustin et al., 2021).

140 The Main Ethiopian Rift is the northernmost section of the intra-continental rifting ~~in~~ East Africa, splitting
141 the ~~not-yet well-individualized~~ not-yet well-individualized Somali plate from Africa (Chorowicz, 2005).
142 Current rifting in the Main Ethiopian Rift is characterized by a narrow rift valley, in which volcanic and
143 tectonic activities are localized and influenced by oblique rifting conditions (Corti, 2009).

144 The Afar triangle is ~~the region~~ where the ~~above-mentioned~~ above-mentioned three rift arms meet (Fig. 3).
145 It is considered ~~as~~ a geological depression as it is an area of low elevation compared to the high Ethiopian
146 plateaus, and thus commonly referred to as the Afar 'depression'. Nevertheless, this term is misleading as
147 the Afar triangle is included within the rifted area and is geologically elevated from the deep bathymetry
148 of the Gulf of Aden and the Red Sea basins. The Afar triangle is mainly floored by Pliocene and younger
149 volcanic rocks, where Miocene volcanic series are exposed along the western margins and at the elevated
150 Danakil block. It comprises many volcanoes that compose axial volcanic ranges (Fig. 2), where the Red Sea
151 side is characterized by transverse volcanic fields and the southern side by central volcanoes (Varet, 2018).
152 Two ~~symmetric~~ magnetic ~~anomalies isochrons~~ have been recognized in the Tendaho graben, ~~which are~~
153 ~~similar to those observed along spreading centers in the Gulf of Aden~~ indicating young oceanization in
154 ~~central Afar~~ (Bridges et al., 2012). ~~These could be associated either with young oceanization, but can also~~
155 ~~be regarded as evidence for~~ or with linear anomalies developed in transitional crust (Ebinger et al., 2017).
156 Structurally, several mega-scale accommodation zones connecting the different rift segments and a triple
157 junction location ~~are~~ is recognized at 11.0°N, 41.6°E at the Tendaho-Goba'ad Discontinuity (e.g, Tesfaye et
158 al., 2003) (Fig. 3).

159 4. Temporal constraints

160 4.1. Flood basalts and uplift

161 Vast efforts were made to study the chemistry and chronology of flood basalts in East Africa (see review
162 by Rooney, 2017). Two phases of extensive flood basalt volcanism are associated with plume-lithosphere
163 interaction (Fig. 4). The early phase is mainly confined to southern Ethiopia and northern Kenya. The timing
164 of this event is poorly constrained to 45-35 Ma (George et al., 1998). The second phase of flood basalt
165 eruptions was more voluminous, more widespread, and shorter-lived. Earliest basalts of this phase date
166 back to 34 Ma near Tana Basin, Ethiopia (Prave et al., 2016) and 31 Ma in western Yemen (Peate et al.,
167 2005) (Fig. 4). The traps accumulated very rapidly, in less than 6 Ma (Coulié et al., 2003), and include
168 tholeiitic to alkaline compositions of asthenosphere mantle source (Mattash et al., 2013). Thick sequences
169 of up to 2 km are observed within a widespread region in Ethiopia and Kenya (Bellieni et al., 1981; Wescott
170 et al., 1999; McDougall and Brown, 2009). It is commonly accepted that these flood basalts are of a [deep-](#)
171 [seated](#)~~deep-seated~~ mantle plume origin (Koppers et al., 2021). However, the mechanism is debatable and
172 may involve multiple plume impingements within a broad upwelling zone connected to the African
173 superplume in the lower mantle (Meshesha and Shinjo, 2008) or a single plume–lithosphere interaction
174 (Rooney, 2017).

175 An elevated topography is associated with the eruption of the flood basalts in Ethiopia. The flood basalts
176 are almost exclusively positioned within the elevated regions of the Ethiopian and Somalian plateaus and
177 the Sarawat Mountains in southwest Yemen (Fig. 1). Dynamic topography component supports up to 1 km
178 of present-day elevation of the Ethiopian and Somalian plateaus, confirming the significant contribution
179 of mantle convection to the regional uplift (Gvirtzman et al., 2016). Although the uplift chronology is not
180 easily resolved, recent studies infer it is a long-term feature, already present before the emplacement of
181 the flood basalts (Sembroni et al., 2016; Faccenna et al., 2019). Regional uplift is estimated to begin before
182 40 Ma, with maximal uplifts between 12 and 28 Ma, reaching an average elevation of 2500 m (Fig. 4)
183 (Sembroni et al., 2016).

184 4.2. Gulf of Aden

185 The beginning of continental rifting in the Gulf of Aden is only approximately known (Bosworth et al.,
186 2005). Estimates mainly rely on the dating of sedimentary sequences, and no recent data ~~was-were~~
187 published. The evidence of rift initiation was summarized by Bosworth et al. (2005). Various sedimentary
188 indications, including onshore outcrops in Yemen (Watchorn et al., 1998) and in Oman (Roger et al., 1989)
189 and offshore wells (Hughes et al., 1991), suggest that rifting in the central and eastern Gulf of Aden began
190 at early to mid-Oligocene, within the Rupelian, i.e., 33.9 - 27.8 Ma. Syn-rift sediments from the central
191 Yemeni margins indicate that rift flank uplift occurred before any significant regional extension. [The](#)
192 [continental](#)~~Continental~~ rifting climax is estimated between 20 and 18 Ma (Watchorn et al., 1998).
193 Radiometric dating indicates that the margins became stable already in the Early Miocene (Bosworth et
194 al., 2005), and rift-to-drift transition is interpreted to occur between ~21.1 and ~17.4 Ma (Watchorn et al.,
195 1998). The seafloor spreading center in the Gulf of Aden is developed along most of its length and is
196 connected to the mid-ocean ridge in the Indian [Ocean](#)~~ocean~~ through the Sheba Ridge (Gillard et al., 2021).
197 In the central Gulf of Aden, magnetic isochrons suggest opening rates of ~27 mm/yr prior to 11 Ma, and a
198 slowdown after 11 Ma (Fig. 4). Chron 5C (purple–stripes in Fig. 3; 16.0 Ma) is present along the Gulf of
199 Aden up to the Shukra al Sheik discontinuity (Fournier et al., 2010). This implies that the spreading center

200 developed ~~very~~ rapidly, perhaps instantaneously, in geological time scales, covering a distance of more
201 than 700 km in less than 1.5 Ma. This fast propagation ceased at the Shukra al Sheik discontinuity (Fig. 3).
202 The youngest magnetic isochrons (2A, 2.6 Ma) ~~are~~ recognized up to longitude 43.9°E in the eastern Gulf
203 of Tadjoura, ~150 km west to the Shukra al Sheik discontinuity, indicating that along this segment, the
204 ridge propagated westward at an average rate of ~11 mm/yr, in the last 16 Ma. Within the Gulf of Tadjoura,
205 no direct evidence of oceanic spreading was reported to our best knowledge.

206 4.3. Red Sea

207 It is not certain when continental rifting in the Red Sea began; however, sedimentary sequences suggest
208 it postdates rifting in the Gulf of Aden by a few million years (Bosworth et al., 2005). Independent evidence
209 suggests that rifting had begun simultaneously along the entire Red Sea at late Oligocene-Early Miocene,
210 ~23 Ma (Plaziat et al., 1998; Szymanski et al., 2016; Stockli and Bosworth, 2018; Morag et al., 2019).
211 Magnetic isochrons associated with seafloor spreading are only known from the southern parts of the Red
212 Sea. However, oceanic lithosphere is probably abundant along most of the basin (Augustin et al., 2021).
213 Chron 3 (4.2 Ma) is only present between latitudes 16° and 18°, while chrons 2A (2.6 Ma) and 2 (1.8 Ma)
214 are present up to latitude 22° (Schettino et al., 2016). Evidence for Chron 5 (10 Ma) in the central Red Sea
215 was recently suggested to mark the beginning of seafloor spreading (Okwokwo et al., 2022). Structural
216 reconstructions, geodetic measurements, and magnetic ~~stripes anomalies~~ suggest opening rates of ~11
217 mm/yr in the central parts of the basin, with an abrupt increase at ~5 Ma (Fig. 4) (Schettino et al., 2018).
218 The southern edges of the magnetic chrons suggest that the ridge rapidly propagated southwards, with
219 rates of ~30 mm/yr, between chrons 3 (4.2 Ma) and 2A (2.6 Ma). ~~However, the rapid propagation was~~
220 ~~halted in the last~~ Since 2.6 Ma, the Red Sea ridge has not propagated southward, probably due to
221 the decrease in angular velocity of Danakil relative to Arabia (Fig. 3) (Fig. 3 ; Schettino et al., 2018).

222 4.4. Main Ethiopian Rift

223 Results from many years of extensive fieldwork (see Corti, 2009 for review) suggest a diachronous
224 development of the different segments of the Main Ethiopian Rift. However, there is no agreement
225 regarding the exact timing of events and even ~~regarding~~ the propagation trend of the rift. Reconstructions
226 based on magnetic anomalies from the Southwest Indian ridge suggest an upper limit for the Nubia-
227 Somalia separation at ~19 Ma, including large uncertainties (DeMets and Merkouriev, 2016) (Fig. 4). There
228 are indications that rifting in East Africa started at the Turkana depression in southern Ethiopia (Varet,
229 2018) and propagated north to Afar (Wolfenden et al., 2004); however, this is still a matter of debate (see
230 figs 42-44 in Corti, 2009). Radiometric dating of structural features indicates that extension commenced
231 at ~11 Ma within the northern Main Ethiopian Rift (Wolfenden et al., 2004).

232 In summary, regional uplift and flood basalt volcanism in Ethiopia preceded the rifting of the Afro-Arabian
233 rift. The rift arms developed at different times, when rifting in the eastern Gulf of Aden started during ~~last~~
234 the late phases of flood basalt volcanism in Ethiopia. Rifting in the Red Sea and ~~in~~ the Main Ethiopian Rift
235 started in a lag of ~5-7 Ma after flood basalt volcanism.

236 5. Data and Methods

237 We used bathymetry and topography data to identify morphotectonic features. To highlight and map the
238 architecture of the margins and axes of the rifts, we applied the Difference of Gaussians method to the

239 topography and the bathymetry grids (Akram et al., 2017). This method allows a fast and accurate edge
240 detection of elevation using active spatial bandpass filtering. We applied luminance coloring to the
241 ~~resultingresulted~~ grid using the open-source image processing software, Gimp.org.

242 To study density-related shallow crustal structures, we used the satellite altimetry-derived vertical gravity
243 gradient (VGG) model of Sandwell et al. (2014), offering 1 arc-min resolution at offshore regions. As higher
244 frequencies are intensified in the spectral power of the VGG, its anomalies are more source-localized and
245 shallow-sensitive than free-air anomalies. To enhance the edges associated with the VGG, we applied a
246 linear 11-colors colormap, further applied transparency to the VGG map, and projected it on a shaded
247 relief (Fig. 5a).

248 To study deeper crustal structures and eliminate ~~the~~ topography effect, we used Bouguer gravity anomaly
249 (BGA), derived from the XGM2019 gravity model (Zingerle et al., 2020), calculated with a grid step of 0.1
250 degrees. The XGM2019 is the most updated global gravity model of the ICGEM and is provided in terms of
251 spherical harmonics up to 2159 ~~degreesdegree~~ (Ince et al., 2019; Zingerle et al., 2020). In addition, we
252 applied a linear 240-colors colormap to enhance BGA structures, further applied transparency to the BGA
253 map, and projected it on a shaded relief (Fig. 5b).

254 To better correlate and discriminate crustal structures and rift features, we considered 1913 earthquake
255 locations from the International Seismological Centre ~~catalogcatalogue~~ with minimum magnitudes above
256 4 ML, recorded between 1964 and 2019. To better infer recent tectonic and volcanic activity, we further
257 considered the locations of Quaternary onshore volcanoes, from the Global Volcanism Program
258 (Smithsonian Institution) and ~~from google~~ ~~Google earth~~ ~~Earth~~ mapping.

259 6. Results

260 6.1. Rift margins

261 The most prominent morphological feature of the rift system is the ~~escarpment sharp cliff~~ along its
262 shoulders. The ~~escarpmentsshoulder cliffs~~ mark the rift margin as they distinguish between (1) uplifted
263 pre-rift rocks of the Arabo-Nubian shield or trap basalts sequences and (2) Quaternary arid fluvial
264 sediments or young volcanic sequences, ~~although several continental crustal fragments are present within~~
265 ~~the Afar Triangle~~. Thus, the ~~escarpmentsshoulder cliffs~~ ~~are very distinctive~~ ~~have a very distinctive~~
266 ~~appearance~~ in the topographical and gravity data. The edge detection analysis of topography and
267 bathymetry data allows us to outline the rift margins (Fig. 6).

268 In the Red Sea, the ~~escarpmentsshoulder cliffs~~ are generally continuous with an average rift width of 440
269 \pm 20 km (calculated perpendicular to the Red Sea axis in the study area), and a general increase in rift width
270 from north to south (Fig. 6b). We identify two segments that mark an abrupt change in rift orientation and
271 rift width: (1) Below latitudes 15.5° on the African margin and 18° on the Arabian margin (segment I in Fig.
272 6), the ~~escarpment rift shoulders~~ deviate from ~~its~~ ~~their~~ general parallel to the Red Sea trend, bending
273 towards the Afar region. The ~~escarpment cliff~~ is characterized by seismic activity from that point on the
274 African side, which is also considered the northern point of the western Afar margins (Zwaan et al., 2020a).
275 (2) Below latitudes 12.5° on the African margin and 15° on the Arabian margin (segment II in Fig. 6), we
276 identify another abrupt change, both in the orientation and the width of the rift. That point on the African
277 margin is the intersection of the Tendaho-Goba'ad Discontinuity with the Western Afar Margins (Tesfaye

278 et al., 2003). We note that these changes are noticeable and similar ~~both~~ on the African and ~~the~~ Arabian
279 sides.

280 In the Gulf of Aden, the ~~escarpments~~~~shoulder cliffs~~ generally follow the trend of the basin. In the western
281 parts, the ~~escarpments~~~~shoulder cliffs~~ are less straight and less continuous than those of the Red Sea and
282 generally reflect the sinistral basin structures. This morphology is well explained by oblique rifting along
283 the Gulf of Aden (Leroy et al., 2013). The average rift width in the study area is 470 ± 45 km (calculated
284 rift-perpendicular), with a general eastward increase (Fig. 6b). We recognize an abrupt change in rift width
285 along three lines (III-V in Fig. 6), which are associated with fracture zones. Along the Somalian margin,
286 prominent sinistral offsets are recognized along lines III and V. This ~~escarpment~~ ~~cliff~~ segment is a
287 morphological continuation of the Tendaho-Goba'ad Discontinuity lineament, and is also prominent in the
288 VGG map (Fig. 5a).

289 Although recognizable in the processed topography map, the rift shoulders are less sharp in the Main
290 Ethiopian Rift (Fig. 6a). They are prominent in the gravity data as they are associated with VGG and BGA
291 highs (see profile A in Fig. 9). In the Afar region, the margins show a funnel shape (Fig. 6a). The distance
292 between the Somalian and Ethiopian ~~escarpments~~ is steadily and monotonically increasing from the Main
293 Ethiopian Rift to the Tendaho-Goba'ad Discontinuity (Fig. 6b), suggesting that this segment is intact and
294 non-disturbed by the other arms of the rift system.

295 In summary, the rift margins of the Red Sea and the Gulf of Aden are interrupted ~~by~~~~with~~ the proximity to
296 the Afar region, whereas the margins of the Main Ethiopian Rift smoothly funnel into the Afar region.

297 6.2. Rift axes

298 Along the Red Sea and the Gulf of Aden basins, the rift axes are distinctively characterized by deep and
299 sharp bathymetric troughs, VGG lows, BGA highs, and intense seismic activity. However, with the proximity
300 to the Afar region, the rift axes change their characteristics.

301 The rift axis along the Red Sea is outlined by a deep and wide axial trough that ends at latitude 14.5° ,
302 approximately 400 km from the triple junction (Fig. 7a). South of latitude 14.5° , we find geophysical
303 evidence that the rift axis is bent, entering the Afar region at the Bay of Beylul (latitude 13.3°): (1) The VGG
304 signature of the Red Sea axis, with highs along the walls of the axial trough and a low above the center
305 (Fig. 7b and profile B). (2) A trail of volcanic islands follows its path (Hanish-Zukur Islands; Fig. 3), ~~and the~~
306 ~~alignments of volcanic cones and vents on the islands are orthogonal to the trail of the islands~~ (Mitchell
307 and Bosworth, (in press); Gass et al., 1973). (3) A general trend of recent onshore magmatism meets this
308 line at the Bay of Beylul (Fig. 3). ~~However, major fault sets are not observed in the onshore area of Beylul~~
309 (Rime et al., 2023). (4) This line ~~also~~ best fits GPS-based rigid block model (Viltres et al., 2020), ~~and is~~
310 ~~supported by the fact that the rotation of Danakil relative to Arabia stopped around $1 \sim 0.3$ Ma~~ (following
311 Schettino et al., 2018 and personal communication). In addition to this ~~bent~~ segment, a typical gravity
312 signature of the rift axis with a central BGA high and VGG picks to its side, is also recognized along the
313 connection of the Red Sea with the Gulf of Aden at Bab al Mandab Strait (latitudes 13.2° to 12.3° ; Fig. 7
314 profile CC'). Nevertheless, this segment is not an active rift axis as no earthquake, volcanic or bathymetrical
315 expression is associated with it, ~~however, diluted activity is also understood by the low and oblique velocity~~
316 ~~of Arabia in this area~~ (Fig. 3).

317 In the Gulf of Aden, there is also a distinct change in the rift axis characteristics, approximately 400 km
318 from the triple junction (Fig. 8). Up to the Shukra al Sheik discontinuity, the Gulf of Aden is a deep basin,
319 reaching depths of more than 1,000 m only a few kilometers from the shore, and has a fragmented axial

320 trough, offset by oblique left-lateral transform faults. West to the Shukra al Sheik discontinuity, the basin
321 is shallow, and the axial trough is very distinct, characterized by deep and sharp morphology. This ~400
322 km long curved ~~axis segment~~~~segment of the axis~~ impales the Afar triangle at the Gulf of Tadjoura (Djibouti).
323 This axial segment has a distinct gravity signature and is characterized by intensive seismic activity, perhaps
324 the most intensive in the rift system, with over 1,000 recorded events with magnitudes ~~s~~ above 4ML (ISC
325 catalogue).

326 In the Main Ethiopian Rift, there are no abrupt changes in the characteristics of the rift valley with the
327 proximity to the Afar triangle (Fig. 9). Instead, the rift valley goes through an elevated dome peaking
328 approximately 400 km from the triple junction (Fig. 9a). The along-strike profile (profile B in Fig. 9) shows
329 that the rift valley reaches altitudes of more than 2,000 m and is associated with a BGA low.

330 In the Afar triangle, the morphology indicates several axial segments, which are also distinctive in the VGG
331 map (Fig. 10). We recognize axial trends in two distinguished and geographically separated regions: (1)
332 southwest to the Tendaho-Goba'ad Discontinuity, a NE trending valley continues the trend of the Main
333 Ethiopian Rift, characterized by distinct central volcanoes along with an axial depression. (2) Northeast to
334 the Tendaho-Goba'ad Discontinuity, typical rift axial morphologies, composed of NW trending short
335 segments along volcanic ranges, are abundant over a 200 km wide zone. Hence, the Afar depression is
336 divided into two morphological regions, in terms of axial trends, parallel to the Main Ethiopian Rift trending
337 region and ~~parallel to~~ the Red Sea trending region.

338 In summary, with the proximity to the Afar depression, the rift axes of the Red Sea and the Gulf Aden are
339 not persistent and drastically change their characteristics ~400 km from the triple junction. In contrast,
340 the axis of the Main Ethiopian Rift is consistent, keeping its trend and characteristics up to the triple
341 junction point.

342 7. Discussion

343 7.1. The architecture of the intersection region

344 The Afar triangle is the intersection region of three rift arms; the Gulf of Aden, the Red Sea, and the Main
345 Ethiopian Rift. Far from the intersection region, the axes and margins of these rifts follow a general parallel
346 trend, suggesting that rigid plate tectonics of the Nubian, Arabian, and Somalian plates controlled their
347 structural development (Garfunkel and Beyth, 2006; Reilinger et al., 2006; Reilinger and McClusky, 2011;
348 Schettino et al., 2018). Within the Afar triangle, southwest to the Tendaho-Goba'ad discontinuity, the rift
349 margins are continuous and smooth, and the axial volcanic range generally continues the trend of the axial
350 valley of the Main Ethiopian Rift, reflecting a sub-perpendicular extension in accordance with the Nubia –
351 Somalia kinematics, and thus, could be regarded as a rigid plate boundary. However, the architecture of
352 the intersection region northeast ~~of~~ the Tendaho-Goba'ad discontinuity is more complex and is not
353 simply resolved by rigid plate kinematics (Garfunkel and Beyth, 2006).

354 Fig. 11 summarizes the rift margins and the axial segments mapped in this study. The rift axes of the Gulf
355 of Aden and the Red Sea abruptly change their characteristics, particularly their trends, with the proximity
356 to the Afar region. Around ~400 km from the triple junction, ~~both~~ the Gulf of Aden and the Red Sea axes
357 deviate from their basin parallel trend, bending towards the third and younger arm of the Main Ethiopian

358 Rift. ~~Within the Afar triangle, The rift margins within Afar,~~ northeast ~~of~~ the Tendaho-Goba'ad
359 discontinuity, the margins are fragmented, and there are multiple, short, and sub-parallel axial segments.

360 In our study, the term "axial segments" inferred is not simply correlated with rift axes, As the geology in
361 this region is quite complex, including several fault and transfer zones, and, exposing pre-rift rock
362 sequences. However, the axial segments mapped in this study in the continental area northeast to the
363 Tendaho-Goba'ad discontinuity is somewhat correlative with rift axes that had been suggested based on
364 field observations (e.g., Rime et al., 2023). Axial segments are generally sub-parallel to the Red Sea axis
365 (Zwaan et al., 2020b) ~~and not to the rift margins~~, which led authors to suggest that this region reflects an
366 evolving discontinuity of the oceanic spreading center in the Red Sea (e.g. Tazieff et al., 1972; Bosworth et
367 al., 2005). ~~However, Although several focal solutions indicated dextral strike-slip motions in this area,~~ we
368 don't find other any evidence for a typical first-order transform connection between the ridge in the Red
369 Sea and the continuation of the northern Afar axial segments, offshore Gulf of Zula. Magnetic stripes in
370 the Red Sea are observed at more than 200 km south of the Gulf of Zula region (Fig. 12-), and the volcanic
371 ridge in the southern Red Sea is very active (Eyles et al., 2018). Although earthquake clusters at latitude
372 16.5° indicate strike-slip solutions, supporting a structural connection to the Red Sea axis, these are
373 abundant throughout the study area (Hofstetter and Beyth, 2003). Alternatively, it is possible to regard
374 the jump between the Red Sea ridge to the axial segments in northeastern Afar as a non-transform
375 discontinuity. However, second-order discontinuities are usually characterized by <30 km offsets, and here
376 the jump is ~~of~~ ~200 km (Macdonald et al., 1984; Carbotte et al., 2016). Thus, we find no circumstantial
377 evidence to regard the axial volcanism in the Afar depression as part of the development of the Red Sea
378 spreading center. This conclusion agrees with the study of Rime et al. (2023), which discusses the
379 geological evidence from Afar.

380 Our analyses ~~suggest~~ highlights that the area northeast to the Tendaho-Goba'ad discontinuity is
381 characterized by diffuse deformation, reflecting a rugged connection of the Red Sea and the Gulf of Aden
382 arms to the Main Ethiopian Rift. Kinematic studies support this view, indicating that microplate rotations
383 and diffuse boundaries significantly influence the structural development of this region. A recent model
384 based on GPS observations (Viltres et al., 2020) reveals a diffuse character of the Danakil - Nubia boundary
385 with inter-rifting deformation over more than 100 km wide zone. The Danakil microplate extends to the
386 Hanish-Zukur Islands at its southern edge (~13.8°N) with no precise/sharp boundary. The Danakil
387 microplate is rotating counterclockwise (Manighetti et al., 2001), while the Ali-Sabieh block, south of the
388 Gulf of Tadjoura, is rotating clockwise (Audin et al., 2004), described as a "saloon-doors" mode of opening
389 (Kidane, 2016).

390 Observations and analog models indicate that strain in Afar is localized in distinct rift segments, which are
391 spread within a broad zone of interaction of the associated plates (Keir et al., 2011; Pagli et al., 2014, 2018;
392 Doubre et al., 2017; Maestrelli et al., 2022). Hence, the architecture of the intersection region of the rift
393 arms discloses a ~150,000 km² complex region, in which diffuse boundaries and microplate rotations link
394 the three rift arms~~the three rift arms are linked by diffuse boundaries and microplate rotations~~ (Fig. 11).
395 Accordingly, a genuinely truly single triple junction point, in the sense of a three-rift arms intersection
396 point, cannot be specified for this system, and multiple triple junctions could be considered (e.g., see
397 tectonic models in Viltres et al., 2020). The difficulty of defining sharp plate boundaries within Afar was
398 discussed in many works (e.g., Barrberi and Varet, 1977 and references therein). Nevertheless, we agree
399 that the intersection point of the Ethiopian rift valley and the Tendaho-Goba'ad Discontinuity could be
400 regarded as the 'main' junction point of the rift system, as the deformation characteristics are most
401 distinctively changed there (Tesfaye et al., 2003).

402 7.2. Spatial constraints in the development of the plume-rift system

403 The architecture of the Afar region allows us to draw two spatial constraints in the development of the
404 plume-rift system:

405 (1) The first is the connection of the Main Ethiopian Rift to the Gulf of Aden - Red Sea rifts by a
406 northeastward propagation. Since the divergence between Nubia-Somalia is sub-vertical to the strike of
407 the northern Main Ethiopian Rift, resolving its propagation direction is quite intangible and conversed
408 (Tesfaye et al., 2003; Wolfenden et al., 2004; Bonini et al., 2005; Keranen and Klemperer, 2008; Abebe et
409 al., 2010). The margins of southeast Afar show symmetric, continuous, and smooth curved trends, from
410 the elevated regions of the Main Ethiopian Rift to the Tendaho-Goba'ad Discontinuity (Fig. 6). With respect
411 to the northeastward trend of the Main Ethiopian rift, the the Somalian margin is curved clockwise, like
412 the Ali-Sabieh sense of rotation (Kidane, 2016), whereas, the Ethiopian margin is curved counterclockwise,
413 like the Danakil sense of rotation (Schult, 1974). This architecture could be understood in terms of fracture
414 mechanics by reorientating reorientation of a propagating fracture near in the vicinity of a pre-existing
415 fracture. Strain analysis indicates that a propagating fracture would curve in-parallel to the pre-existing
416 fracture under a tensional stress field due to free surface boundary conditions induced by the open pre-
417 existing fracture (Dyer, 1988). Thus, this macro scale architecture may express a smooth linkage of the
418 Main Ethiopian Rift to the pre-existing Gulf of Aden-Red Sea rifts by a northeastward propagation. Hence,
419 this implies that a triple junction formed at a late stage, when all the three arms were already significantly
420 developed. This conclusion agrees with structural geochronology within the northern Main Ethiopian Rift,
421 showing that extension in the northern Main Ethiopian rift commenced at 11 Ma (Wolfenden et al., 2004).

422 (2) The second spatial constraint is abandoning an abandonment of an early tectonic connection between
423 the Red Sea and the Gulf of Aden through the Bab al-Mandab Strait. As the VGG and neovolcanic activity
424 indicate that the Red Sea axis currently enters Afar at the Bay of Beylul (see section 6.2), we find arguments
425 for an earlier tectonic connection between the Red Sea and the Gulf of Aden through Bab al-Mandab Strait:
426 (i) Below latitude 13.2° and up to the connection to the Gulf of Aden (at latitude 12.3°), the gravity data
427 shows typical rift axis characteristics, with BGA high and VGG picks to its side (Fig. 7 and Fig. 8; see section
428 6.2). (ii) The submarine Submarine channel north to the Hanish Island (latitude 13.4°) has shows no
429 association with with the modern water currents and is best may be explained by subsurface rift structures
430 (Mitchell and Sofianos, 2018). (iii) This is the straight continuation of the trend of the Red Sea axis, along
431 which the basins are curvly connected (Fig. 1). Thus, it is reasonable that it was also the tectonic connection
432 in the early stages of rift development. Likewise, reconstructions suggest that the Danakil microplate
433 started to rotate in Oligocene the Middle Miocene (~10 Ma), when Arabia was already separated from
434 Africa (Collet et al., 2000; Schettino et al., 2016; Rime et al., 2023). Those reconstructions shows shows that
435 until that time, the divergence was focused along the seaway at the southernmost Red Sea. This suggests
436 that the present deviation from the basin parallel trend of the rift axes at the tip of the Gulf of Aden and
437 of the Red Sea marks a tectonic reorganization in this region.

438 By adopting the fracture propagation analog postulated here for the northeastward propagation of the
439 Main Ethiopian Rift, it follows that the abandonment of the tectonic connection between the Red Sea and
440 the Gulf of Aden happens as a response to the new stress conditions in Afar. Rime et al. (2023) suggest
441 that the deposition of lacustrine sediments in Afar (Chorora Fm) marks the development of the Main
442 Ethiopian Rift in Afar. They point out that these sediments were deposited roughly at the same time to the
443 individualization of the Danakil Block, and thus to the reduction in the tectonic activity of the southernmost
444 Red Sea rift.

445 These two spatial constraints, ~~the connection of the Main Ethiopian Rift to the Gulf of Aden and to the Red~~
446 ~~Sea by a northeastward propagation, and, the abandonment of an early tectonic connection between the~~
447 ~~Red Sea and the Gulf of Aden,~~ indicate that the onset of the triple junction happened at a late stage when
448 the three rift arms were already developed and the Red Sea was tectonically connected to the Gulf of
449 Aden, far (~250 km) from the present-day triple junction (Fig. 13). The onset of the triple junction marks a
450 tectonic reorganization and microplate formation. As a result, the Gulf of Aden and the Red Sea arms are
451 not smoothly connected to the Main Ethiopian Rift, and a vast area of diffuse and complex deformation
452 developed within the intersection region.

453 7.3. Mechanisms for plume-rift association

454 The temporal constraints regarding the development of the plume-rift features, summarized in section 4,
455 together with the two spatial constraints inferred in this study, allow us to examine the causal relationship
456 between the activity of the Afar plume and rifting. Our insights suggest that neither 'active' nor 'passive'
457 rifting mechanisms are solely consistent with the observation. Passive rifting models fail to explain the
458 plume-rift association ~~mainly~~ ~~mostly~~ because the flood basalt volcanism cannot be attributed to passively
459 rising asthenospheric mantle beneath a stretched and thinned lithosphere, as dynamic uplift in Ethiopia
460 was shown to be a long-lasting process, prior to flood basalts volcanism (Sembroni et al., 2016). Hence,
461 rifting and associated subsidence ~~are~~ ~~is~~ subsequent to flood basalts volcanism (Fig. 4). The estimations of
462 ~1 km elevation ~~before~~ ~~prior to~~ flood basalts (Fig. 4) coincide with active plume-head predictions (Campbell
463 and Griffiths, 1990). Moreover, the passive model does not ~~explain~~ ~~provide an explanation for~~ why a triple
464 junction is located within the flood basalts area, as rifting in the Red Sea and Gulf of Aden are at an oblique
465 angle to the former sutures (Buiter and Torsvik, 2014).

466 ~~On the other hand, active models~~ ~~Active models, on the other hand,~~ are not in line with the progressive
467 development of the rifts, mainly because the flood basalts ~~—~~region cannot be considered a center or a
468 nucleus, from which rift arms spread, as expected in an actively generated triple junction. ~~Numerous~~
469 ~~studies noted that~~ ~~The incompatibility of the tectonic development of the Afar region is not compatible~~
470 ~~with to a simplified model of rift arms that simultaneously spread away from a triple junction, was noted~~
471 ~~by numerus studies~~ (see Section 5.2 in Rime et al., 2023 for a review). The ~~inset of a~~ triple junction was the
472 last feature to develop in the system, by the propagation of the Main Ethiopian Rift towards Afar, followed
473 by a tectonic reorganization including the abandonment of a former tectonic connection between the Red
474 Sea and the Gulf of Aden. By this time, the rift arms ~~had~~ ~~were~~ already developed, and ~~the~~ break-up ~~had~~ ~~was~~
475 already ~~been~~ accomplished between Africa and Arabia. This tectonic reorganization cannot be attributed
476 to the development of gravitational potential by the plume head (Hill, 1991), as it occurred millions of
477 years after flood basalts magmatism. That rules out the possibility that ~~the arrival of the Afar plume~~
478 ~~generated the onset of the triple junction~~ ~~the onset of the triple junction was generated by the arrival of~~
479 ~~the Afar plume,~~ as more than 20 Ma separate these events ~~and,~~ ~~and as~~ the rift arms did not spread from
480 the plume region.

481 We propose a scenario in which rifting was triggered by a plume-induced plate rotation (Fig. 2c). Numerical
482 simulations suggest that horizontal asthenospheric flows due to the arrival of a plume-~~head~~ at the base
483 of the lithosphere induce a plume-push force that can accelerate plates by several cm yr^{-1} (van Hinsbergen
484 et al., 2011, 2021; Pusok and Stegman, 2020). In this scenario, flood basalt volcanism would be
485 synchronous to an abrupt plate speed-up and thus to new remote stress conditions. In the case of the
486 Indian plate, at least two episodes of massive flood basalt volcanism, Morondava LIP (~94 Ma) and Deccan
487 traps (67 Ma), are associated with ~~plume-derived~~ ~~plume-derived~~ plate acceleration, and a drastic change

488 in the tectonic framework (van Hinsbergen et al., 2011, 2021; Cande and Stegman, 2011; Pusok and
489 Stegman, 2020). Further, torque balance modeling suggests that horizontal plume-push can force a
490 significant plate rotation and, consequently, ~~initiate the initiation of~~ new plate boundaries (van Hinsbergen
491 et al., 2021).

492 In the Afro-Arabian rift, indeed new plate boundaries formed after the arrival of the large Afar plume and
493 a significant plate rotation of Arabia around a nearby pole characterizes the Arabian continent (Joffe and
494 Garfunkel, 1987; Viltres et al., 2022). Magnetic ~~stripes anomalies~~ and structural reconstructions suggest
495 that the rotation around a nearby pole already ~~characterized~~ characterizes Arabia since the Oligocene
496 (Fournier et al., 2010; Schettino et al., 2018). Additionally, the beginning of intensive volcanism in the
497 north-western Arabian plate (Harrat Ash Shaam) at Late Oligocene (Ilani et al., 2001), reflects ~~ing~~ a change
498 in mantle-crust interaction and ~~in-~~intracontinental extension within the Arabian plate, adjacent to the
499 arrival of Afar plume (Garfunkel, 1989). In the ~~is large~~ Harrat Ash Shaam volcanic field, diking directions
500 from Miocene to recent ages record the rotation of Arabia (Giannerini et al., 1988), suggesting that already
501 during the first stages of volcanism the Arabian plate was rotating around a nearby pole.

502 The arrival of the Afar plume was also accompanied by a slowdown of Africa (Le Pichon and Gaulier, 1988).
503 By this time, Africa collided with Eurasia in the west, explaining its slowdown (Jolivet and Faccenna, 2000)
504 and ~~its~~ increased intraplate volcanism (Burke, 1996). However, this collision of Africa and Eurasia cannot
505 simply resolve the change in the rotation of Arabia as the Arabian continent collided with Eurasia ~~not~~
506 earlier than ~18 Ma (Su and Zhou, 2020), although some authors suggested that asymmetrical along-
507 trench entrance of continental material could lead to an intraplate extension similar to those that
508 generated the Africa-Arabia break-up (Bellahsen et al., 2003). Faccenna et al. (2013) already showed that
509 plume-push from the Afar area resolves the present-day plate kinematics in the ~~Middle East~~ middle-east,
510 particularly the anti-clockwise toroidal pattern of the Arabia–Anatolia–Aegean system. The importance of
511 active upwelling in Afar to lateral mantle flow below Arabia is also illustrated by shear-wave splitting,
512 indicating a general N-S anisotropy in the mantle (Qaysi et al., 2018). Stamps et al. (2014) calculated the
513 current driving forces for the Nubia-Somalia divergence and found that gravitational potential energy is
514 the most significant force, stronger by an order of magnitude than forces from basal shear tractions of
515 mantle convection. They point out that the gravitational potential energy is sufficient to sustain present-
516 day rifting in East Africa but not to initiate rupture of continental lithosphere. In the case of the Arabian
517 plate, basal shear tractions are expected to be higher due to the orientation of northward-directed mantle
518 flow (Faccenna et al., 2013).

519 If ~~the Afar plume induced the rotation of Arabia around a nearby pole~~ ~~the rotation of Arabia around a~~
520 ~~nearby pole was induced by the Afar plume~~, then it is understood how the Gulf of Aden and the Red Sea
521 rifts developed after a regional uplift and flood basalt volcanism but still geometrically developed by the
522 new regional stress field and structural inheritance (Autin et al., 2013; Bosworth and Stockli, 2016). It also
523 ~~explains~~ provides an explanation of why the trace of the rifts intersect within the plume region as the
524 lithosphere in this region was weakened by the hot plume material (François et al., 2018). Finally, it
525 explains the delayed development of the Main Ethiopian Rift and the late onset of the Afar triple junction
526 by its northwestward propagation, as these were controlled by the slower kinematics of the Somalian plate
527 rather than dynamic forces. In this manner, ‘active’ and ‘passive’ mechanisms are coupled and have ~~a~~
528 positive feedback, allowing a close occurrence of flood basalt ~~s~~ volcanism and continental break-up,
529 alongside a passive style of rifting.

530 8. Summary and Conclusions

531 We reviewed the geologic setting of the Afro-Arabian rift, in which vast regions of flood basalts and ~~an~~
532 ongoing continental break-up are superimposed, aiming to infer a causal relationship between the activity
533 of the deep-seated Afar plume and crustal break-up. We explored the intersection region wherein which
534 the Gulf of Aden, the Red Sea, and the Main Ethiopian Rift form an R-R-R triple junction, separating the
535 large Cenozoic ~~plume-related~~plume-related flood basalt series in Ethiopia and Yemen. We provide a new
536 synthesis and interpretation ~~of~~of modern geophysical datasets, including topography, bathymetry, gravity,
537 magnetic anomalies, earthquakes, and volcano distribution, to map the margins and axes of the rift arms.

538 We highlight key differences in the terminations of the Gulf of Aden and the Red Sea arms, which are rough
539 and irregular, versus the symmetric, continuous, and smooth architecture of the Main Ethiopian Rift. The
540 architecture of the intersection regions allows us to infer two tempo-spatial constraints in the
541 development of the rifts: (1) the connection of the Main Ethiopian Rift to the Gulf of Aden and to the Red
542 Sea by its northeastward propagation, and, (2) the abandonment of an early tectonic connection between
543 the Red Sea and the Gulf of Aden. These suggest a progressive development of the intersection area,
544 including a broad region of diffuse deformation and recent tectonic reorganization. The onset of the triple
545 junction was the last feature to develop in the plume-rift system, after all rift arms were sufficiently
546 developed and the break-up was accomplished.

547 This progressive development ~~does not align~~is not in line with the classic active rifting model, which
548 predicts a plume-generated triple junction at the locus of the rift, from which the rifts develop.
549 Nevertheless, the classic passive rifting model fails to explain the chronological evidence, as flood basalts
550 probably erupted on elevated topography before rifting started. We discuss a scenario of plume-induced
551 plate rotation in which the arrival of the Afar plume triggered the rotation of Arabia around a nearby
552 ~~polethe rotation of Arabia around a nearby pole was triggered by the arrival of the Afar plume. We, and~~
553 demonstrate that the rotation of Arabia around a nearby pole characterizes the system since the Oligocene
554 ~~and reflects observed mantle flows below Arabia~~. We suggest that this scenario better explains the
555 progressive development of the plume-rift system in the Afro-Arabian rift.

556 9. Data availability

557 The bathymetry and topography data used in this study was retrieved from GEBCO Compilation Group
558 (2021), available at https://www.gebco.net/data_and_products/gridded_bathymetry_data/#area.

559 The VGG data used in this study is available at https://topex.ucsd.edu/grav_outreach/.

560 The BGA data used in this study is available at <http://icgem.gfz-potsdam.de/calgrid>; model XGM2019e-
561 2159, 'gravity_anomaly_bg'.

562 Earthquake data was retrieved from the International Seismological Centre (2020), On-line Bulletin,
563 <https://doi.org/10.31905/D808B830>.

564 Quaternary onshore volcano locations were retrieved from the Global Volcanism Program, Smithsonian
565 Institution, available at https://volcano.si.edu/volcanolist_holocene.cfm.

566 [Magnetic anomalies data is available at](https://figshare.com/articles/dataset/Transcurrent_Regimes_During_Rotational_Rifting_New_Insights_from_Magnetic_Anomalies_in_the_Red_Sea/14743272)
567 [https://figshare.com/articles/dataset/Transcurrent Regimes During Rotational Rifting New Insights f](https://figshare.com/articles/dataset/Transcurrent_Regimes_During_Rotational_Rifting_New_Insights_from_Magnetic_Anomalies_in_the_Red_Sea/14743272)
568 [rom Magnetic Anomalies in the Red Sea/14743272](https://figshare.com/articles/dataset/Transcurrent_Regimes_During_Rotational_Rifting_New_Insights_from_Magnetic_Anomalies_in_the_Red_Sea/14743272)

569 10. Author contribution

570 RI carried out the study and wrote and revised the original draft of this paper. PH and NA provided a
571 conceptual assistance, helped in writing and reviewed the manuscript. JE mentored the study, took care
572 of administration, and reviewed the manuscript.

573 11. Competing interests

574 The contact author has declared that neither of the authors has any competing interests.

575 12. Acknowledgments

576 This work was supported by the grants from Minerva Fellowship to R. I. [We thank Neil Mitchell and](#)
577 [Valentin Rime for their helpful discussion throughout the open discussion process. We wish to thank](#)
578 [Antonio Schettino and Derek Keir for their review which helped improving the manuscript.](#)

579 13. Figure captions

580 **Fig. 1.** Elevation map of the study area, showing the general plate tectonic configuration (from USGS and
581 from Viltres et al. (2020) in the Afar region) and Cenozoic volcanics (modified from Varet, 1978; Davison
582 et al., 1994; Beyene and Abdelsalam, 2005; Bosworth and Stockli, 2016) Black arrows indicate GPS
583 velocities in respect to Nubia (modified from Reilinger et al., 2006).

584 **Fig. 2.** Schematic mechanisms for plume-rift association in the Afro-Arabian rift. (a) Active mechanism, in
585 which rifting results from the actively rising head of the Afar plume. In this mechanism impinging and
586 eroding the base of the lithosphere prompt uplift and decompression melting and flood basalts volcanism.
587 These introduce internal extensional forces and ultimately lead to break-up. (b) Passive mechanism, in
588 which rifting is initiated solely by the remote stresses, regardless of underlying Afar plume. In this
589 mechanism the production of massive volcanism is allowed when the thinned and stretched lithosphere
590 is underlaid by the thermal anomaly in the mantle. Flood basalts volcanism is generated by passively rising
591 decompression melting of hot asthenospheric mantle. (c) Plume-induced plate rotation, in which lateral
592 forces, induced by the arrival of the Afar plume head, add up to the remote stresses to change the plate
593 kinematics. In this mechanism flood basalts volcanism is actively controlled, however, rifting is triggered
594 by the new plate kinematics.

595 **Fig. 3.** Map of the Afar region showing magnetic isochrons (modified from Fournier et al., 2010; Bridges et
596 al., 2012; Schettino et al., 2016), earthquake locations (from ISC catalog), Holocene onshore volcano
597 locations (from GVP catalog and Viltres et al. (2020)) and recent volcanism (modified from Keir et al., 2013).

598 **Fig. 4.** Elevation of the Ethiopian–Yemen plateau (after Sembroni et al., 2016; Faccenna et al., 2019),
599 volcanic episodes and opening rates of the rift arms (modified from Fournier et al., 2010; DeMets and
600 Merkouriev, 2016; Schettino et al., 2018). Dashed lines indicate estimations from geological observations
601 and solid lines from magnetic isochrons.

602 **Fig. 5.** Gravity data of the Afar region. (a) Vertical gravity gradient from Sandwell et al. (2014). Bouguer
603 anomaly model from ICGEM, XGM2019e (Zingerle et al., 2020).

604 **Fig. 6.** (a) Difference of Gaussians applied to topography and bathymetry showing rift margins (black lines).
605 White dashed lines indicate peaks in rift width. TGD is the Tendaho-Goba’ad Discontinuity. SSD is the
606 Shukra al Sheik discontinuity. Black dots indicate earthquake locations (ISC catalog). (b) Rift widths,
607 calculated in rift-perpendicular directions.

608 **Fig. 7.** Bathymetry (a), vertical gravity gradient (b) and Bouguer anomaly (c) in the southern Red Sea. Black
609 dots indicate earthquake locations (ISC catalog). (d) Profiles across rift axis.

610 **Fig. 8.** Bathymetry (a), vertical gravity gradient (b) and Bouguer anomaly (c) in the Western Gulf of Aden.
611 Black dots indicate earthquake locations (ISC catalog). (d) Profiles across rift axis.

612 **Fig. 9.** Topography (a), vertical gravity gradient (b) and Bouguer anomaly (c) in the northern Main Ethiopian
613 Rift. Black dots indicate earthquake locations (ISC catalog). (d) Profiles across (AA’) and along (BB’) the rift
614 valley.

615 **Fig. 10.** Topography (a), vertical gravity gradient (b) and Bouguer anomaly (c) in the Afar triangle. Black
616 dots indicate earthquake locations (ISC catalog). TGD is the Tendaho-Goba’ad Discontinuity. (d) Profiles
617 SW (AA’) and NE (BB’) to the TGD.

618 **Fig. 11.** Rift margins (solid white lines) and axial segments (long dashed black lines) in the Afar region. Black
619 dots indicate earthquake locations (ISC catalog). TGD is the Tendaho-Goba’ad Discontinuity.

620 **Fig. 12.** Tilt-angle derivative map of magnetic anomalies, projected on a shaded relief after Issachar et al.
621 (2022). Purple colors represent positive angles and green colors represent negative angles. White dashed
622 lines indicate magnetic stripes (Schettino et al., 2016).

623 **Fig. 13.** Synthesis of the progressive development of the rift intersections.

624 14. References

- 625 Abebe, T., Balestrieri, M.L., and Bigazzi, G., 2010, The Central Main Ethiopian Rift is younger than 8 Ma:
626 confirmation through apatite fission-track thermochronology:, doi:10.1111/j.1365-
627 3121.2010.00968.x.
- 628 Akram, F., Garcia, M.A., and Puig, D., 2017, Active contours driven by difference of Gaussians: Scientific
629 Reports, v. 7, p. 1–15, doi:10.1038/s41598-017-14502-w.
- 630 Anderson, D.L., 2005, Large Igneous Provinces, Delamination, and Fertile Mantle: Elements, v. 1, p. 271–
631 275, doi:10.2113/gselements.1.5.271.
- 632 Anderson, D.L., 1994, The sublithospheric mantle as the source of continental flood basalts; the case
633 against the continental lithosphere and plume head reservoirs: Earth and Planetary Science Letters,

634 v. 123, p. 269–280, doi:[https://doi.org/10.1016/0012-821X\(94\)90273-9](https://doi.org/10.1016/0012-821X(94)90273-9).

635 Audin, L., Quidelleur, X., Coulié, E., Courtillot, V., Gilder, S., Manighetti, I., Gillot, P.Y., Tapponnier, P., and
636 Kidane, T., 2004, Palaeomagnetism and K-Ar and 40 Ar/39 Ar ages in the Ali Sabieh area (Republic of
637 Djibouti and Ethiopia): Constraints on the mechanism of Aden ridge propagation into southeastern
638 Afar during the last 10 Myr: *Geophysical Journal International*, v. 158, p. 327–345,
639 doi:10.1111/j.1365-246X.2004.02286.x.

640 Augustin, N., van der Zwan, F.M., Devey, C.W., and Brandsdóttir, B., 2021, 13 million years of seafloor
641 spreading throughout the Red Sea Basin: *Nature Communications*, v. 12, p. 1–10,
642 doi:10.1038/s41467-021-22586-2.

643 Autin, J., Bellahsen, N., Leroy, S., Husson, L., Beslier, M.O., and d’Acremont, E., 2013, The role of structural
644 inheritance in oblique rifting: Insights from analogue models and application to the Gulf of Aden:
645 *Tectonophysics*, v. 607, p. 51–64, doi:10.1016/J.TECTO.2013.05.041.

646 Barrberi, F., and Varet, J., 1977, Volcanism of Afar: Small-scale plate tectonics implications: *GSA Bulletin*,
647 v. 88, p. 1251–1266, doi:10.1130/0016-7606(1977)88<1251:VOASPT>2.0.CO;2.

648 Bellahsen, N., Faccenna, C., Funicello, F., Daniel, J.M., and Jolivet, L., 2003, Why did Arabia separate from
649 Africa? Insights from 3-D laboratory experiments: *Earth and Planetary Science Letters*, v. 216, p. 365–
650 381, doi:10.1016/S0012-821X(03)00516-8.

651 Bellahsen, N., Husson, L., Autin, J., Leroy, S., and D’Acremont, E., 2013, The effect of thermal weakening
652 and buoyancy forces on rift localization: Field evidences from the Gulf of Aden oblique rifting:
653 *Tectonophysics*, v. 607, p. 80–97, doi:10.1016/j.tecto.2013.05.042.

654 Bellieni, G., Visentin, E.J., Zanettin, B., Piccirillo, E.M., Radicati di Brozolo, F., and Rita, F., 1981, Oligocene
655 transitional tholeiitic magmatism in Northern turkana (Kenya): Comparison with the Coeval Ethiopian
656 volcanism: *Bulletin Volcanologique*, v. 44, p. 411–427, doi:10.1007/BF02600573.

657 Beyene, A., and Abdelsalam, M.G., 2005, Tectonics of the Afar Depression: A review and synthesis: *Journal*
658 *of African Earth Sciences*, v. 41, p. 41–59, doi:10.1016/j.jafrearsci.2005.03.003.

659 Bonini, M., Corti, G., Innocenti, F., Manetti, P., Mazzarini, F., Abebe, T., and Pecskay, Z., 2005, Evolution of
660 the Main Ethiopian Rift in the frame of Afar and Kenya rifts propagation: v. 24,
661 doi:10.1029/2004TC001680.

662 Bosworth, W., 2015, Geological evolution of the Red Sea: historical background, review, and synthesis, *in*
663 *In The Red Sea*, Springer, Berlin, Heidelberg, p. 45–78, doi:10.1007/978-3-662-45201-1.

664 Bosworth, W., Huchon, P., and McClay, K., 2005, The Red Sea and Gulf of Aden Basins: *Journal of African*
665 *Earth Sciences*, v. 43, p. 334–378, doi:10.1016/j.jafrearsci.2005.07.020.

666 Bosworth, W., and Stockli, D.F., 2016, Early magmatism in the greater Red Sea rift: Timing and significance:
667 *Canadian Journal of Earth Sciences*, v. 53, p. 1158–1176, doi:10.1139/cjes-2016-0019.

668 Bridges, D.L., Mickus, K., Gao, S.S., Abdelsalam, M.G., and Alemu, A., 2012, Magnetic stripes of a
669 transitional continental rift in Afar: *Geology*, v. 40, p. 203–206, doi:10.1130/G32697.1.

670 Bryan, S.E., and Ferrari, L., 2013, Large igneous provinces and silicic large igneous provinces: Progress in
671 our understanding over the last 25 years: *GSA Bulletin*, v. 125, p. 1053–1078, doi:10.1130/B30820.1.

672 Buiter, S.J.H., and Torsvik, T.H., 2014, A review of Wilson Cycle plate margins: A role for mantle plumes in
673 continental break-up along sutures? *Gondwana Research*, v. 26, p. 627–653,
674 doi:10.1016/J.GR.2014.02.007.

- 675 Burke, K., 1996, The African Plate: South African Journal of Geology, v. 99, p. 341–409, doi:10.10520/EJC-
676 942801F20.
- 677 Burke, K., and Dewey, J.F., 1973, Plume-generated triple junctions: key indicators in applying plate
678 tectonics to old rocks: The Journal of Geology, v. 81, p. 406–433,
679 doi:https://doi.org/10.1086/627882.
- 680 Campbell, I.H., and Griffiths, R.W., 1990, Implications of mantle plume structure for the evolution of flood
681 basalts: Earth and Planetary Science Letters, v. 99, p. 79–93, doi:10.1016/0012-821X(90)90072-6.
- 682 Cande, S.C., and Stegman, D.R., 2011, Indian and African plate motions driven by the push force of the
683 Réunion plume head: Nature, v. 475, p. 47–52, doi:10.1038/nature10174.
- 684 Carbotte, S.M., Smith, D.K., Cannat, M., and Klein, E.M., 2016, Tectonic and magmatic segmentation of the
685 Global Ocean Ridge System: A synthesis of observations, *in* Geological Society Special Publication,
686 Geological Society of London, v. 420, p. 249–295, doi:10.1144/SP420.5.
- 687 Chatterjee, S., Goswami, A., and Scotese, C.R., 2013, The longest voyage: Tectonic, magmatic, and
688 paleoclimatic evolution of the Indian plate during its northward flight from Gondwana to Asia:
689 Gondwana Research, v. 23, p. 238–267, doi:10.1016/j.gr.2012.07.001.
- 690 Chorowicz, J., 2005, The East African rift system: Journal of African Earth Sciences, v. 43, p. 379–410,
691 doi:10.1016/j.jafrearsci.2005.07.019.
- 692 Collet, B., Taud, H., Parrot, J.F., Bonavia, F., and Chorowicz, J., 2000, A new kinematic approach for the
693 Danakil block using a Digital Elevation Model representation: Tectonophysics, v. 316, p. 343–357,
694 doi:10.1016/S0040-1951(99)00263-2.
- 695 Corti, G., 2009, Continental rift evolution: From rift initiation to incipient break-up in the Main Ethiopian
696 Rift, East Africa: Earth-Science Reviews, v. 96, p. 1–53, doi:10.1016/j.earscirev.2009.06.005.
- 697 Coulié, E., Quidelleur, X., Courtillot, V., Lefèvre, J.C., and Chiesa, S., 2003, Comparative K-Ar and Ar/Ar
698 dating of Ethiopian and Yemenite Oligocene volcanism: Implications for timing and duration of the
699 Ethiopian traps: Earth and Planetary Science Letters, v. 206, p. 477–492, doi:10.1016/S0012-
700 821X(02)01089-0.
- 701 Courtillot, V., Jaupart, C., Manighetti, I., Tapponnier, P., and Besse, J., 1999, On causal links between flood
702 basalts and continental breakup: Earth and Planetary Science Letters, v. 166, p. 177–195,
703 doi:10.1016/S0012-821X(98)00282-9.
- 704 Davison, I. et al., 1994, Geological evolution of the southeastern Red Sea Rift margin, Republic of Yemen:
705 Geological Society of America Bulletin, v. 106, p. 1474–1493, doi:10.1130/0016-
706 7606(1994)106<1474:GEOTSR>2.3.CO;2.
- 707 DeMets, C., and Merkouriev, S., 2016, High-resolution estimates of Nubia-Somalia plate motion since 20
708 Ma from reconstructions of the Southwest Indian Ridge, Red Sea and Gulf of Aden: Geophysical
709 Journal International, v. 207, p. 317–332, doi:10.1093/gji/ggw276.
- 710 Doubre, C. et al., 2017, Current deformation in Central Afar and triple junction kinematics deduced from
711 GPS and InSAR measurements: Geophysical Journal International, v. 208, p. 936–953,
712 doi:10.1093/gji/ggw434.
- 713 Duclaux, G., Huismans, R.S., and May, D.A., 2020, Rotation, narrowing, and preferential reactivation of
714 brittle structures during oblique rifting: Earth and Planetary Science Letters, v. 531, p. 115952,
715 doi:10.1016/j.epsl.2019.115952.
- 716 Dyer, R., 1988, Using joint interactions to estimate paleostress ratios: Journal of Structural Geology, v. 10,

717 p. 685–699, doi:10.1016/0191-8141(88)90076-4.

718 Ebinger, C.J., Keir, D., Bastow, I.D., Whaler, K., Hammond, J.O.S., Ayele, A., Miller, M.S., Tiberi, C., and
719 Hautot, S., 2017, Crustal Structure of Active Deformation Zones in Africa: Implications for Global
720 Crustal Processes: *Tectonics*, v. 36, p. 3298–3332, doi:https://doi.org/10.1002/2017TC004526.

721 Ernst, R.E., 2014, *Large igneous provinces*: Cambridge University Press.

722 Eyles, J.H.W., Illsley-Kemp, F., Keir, D., Ruch, J., and Jónsson, S., 2018, Seismicity Associated With the
723 Formation of a New Island in the Southern Red Sea: *Frontiers in Earth Science*, v. 6, p. 1–10,
724 doi:10.3389/feart.2018.00141.

725 Faccenna, C., Becker, T.W., Jolivet, L., and Keskin, M., 2013, Mantle convection in the Middle East:
726 Reconciling Afar upwelling, Arabia indentation and Aegean trench rollback: *Earth and Planetary
727 Science Letters*, v. 375, p. 254–269, doi:10.1016/J.EPSL.2013.05.043.

728 Faccenna, C., Glišović, P., Forte, A., Becker, T.W., Garzanti, E., Sembroni, A., and Gvirtzman, Z., 2019, Role
729 of dynamic topography in sustaining the Nile River over 30 million years: *Nature Geoscience*, v. 12,
730 p. 1012–1017, doi:10.1038/s41561-019-0472-x.

731 Forsyth, D., and Uyeda, S., 1975, On the relative importance of the driving forces of plate motion:
732 *Geophysical Journal International*, v. 43, p. 163–200.

733 Fournier, M. et al., 2010, Arabia-Somalia plate kinematics, evolution of the Aden-OwenCarlsberg triple
734 junction, and opening of the Gulf of Aden: *Journal of Geophysical Research: Solid Earth*, v. 115, p. 1–
735 24, doi:10.1029/2008JB006257.

736 François, T., Koptev, A., Cloetingh, S., Burov, E., and Gerya, T., 2018, Plume-lithosphere interactions in
737 rifted margin tectonic settings: Inferences from thermo-mechanical modelling: *Tectonophysics*, v.
738 746, p. 138–154, doi:10.1016/j.tecto.2017.11.027.

739 Frizon De Lamotte, D., Fourdan, B., Leleu, S., Leparmentier, F., and De Clarens, P., 2015, Style of rifting and
740 the stages of Pangea breakup: *Tectonics*, v. 34, p. 1009–1029, doi:10.1002/2014TC003760.

741 Fromm, T., Planert, L., Jokat, W., Ryberg, T., Behrmann, J.H., Weber, M.H., and Haberland, C., 2015, South
742 Atlantic opening: A plume-induced breakup? *Geology*, v. 43, p. 931–934, doi:10.1130/G36936.1.

743 Garfunkel, Z., 1989, Tectonic setting of phanerozoic magmatism in Israel: *Israel journal of earth-sciences*,
744 v. 38, p. 51–74.

745 Garfunkel, Z., and Beyth, M., 2006, Constraints on the structural development of Afar imposed by the
746 kinematics of the major surrounding plates: *Geological Society Special Publication*, v. 259, p. 23–42,
747 doi:10.1144/GSL.SP.2006.259.01.04.

748 Gass, I.G., Mallick, D.I.J., and Cos, K.G., 1973, Volcanic islands of the Red Sea: *Journal of the Geological
749 Society*, v. 129, p. 275–309, doi:10.1144/gsjgs.129.3.0275.

750 GEBCO Compilation Group, 2021, The GEBCO_2019 Grid: a continuous terrain model of the global oceans
751 and land; doi:10.5285/c6612cbe-50b3-0cff-e053-6c86abc09f8f.

752 Geoffroy, L., 2005, Volcanic passive margins: *Comptes Rendus Geoscience*, v. 337, p. 1395–1408,
753 doi:10.1016/J.CRTE.2005.10.006.

754 George, R., Rogers, N., and Kelley, S., 1998, Earliest magmatism in Ethiopia: Evidence for two mantle
755 plumes in one flood basalt province: *Geology*, v. 26, p. 923–926, doi:10.1130/0091-
756 7613(1998)026<0923:EMIEEF>2.3.CO;2.

757 Giannerini, G., Campredon, R., Feraud, G., and Abou Zakhem, B., 1988, Deformations intraplaques et

758 volcanisme associe; exemple de la bordure NW de la plaque Arabique au Cenozoique: Bulletin de la
759 Société Géologique de France, v. IV, p. 937–947, doi:10.2113/gssgfbull.IV.6.937.

760 Gillard, M., Leroy, S., Cannat, M., and Sloan, H., 2021, Margin-to-Margin Seafloor Spreading in the Eastern
761 Gulf of Aden: A 16 Ma-Long History of Deformation and Magmatism from Seismic Reflection, Gravity
762 and Magnetic Data: *Frontiers in Earth Science*, v. 9, p. 628, doi:10.3389/feart.2021.707721.

763 Gvirtzman, Z., Faccenna, C., and Becker, T.W., 2016, Isostasy, flexure, and dynamic topography:
764 *Tectonophysics*, v. 683, p. 255–271, doi:10.1016/j.tecto.2016.05.041.

765 Hill, R.I., 1991, Starting plumes and continental break-up: *Earth and Planetary Science Letters*, v. 104, p.
766 398–416, doi:10.1016/0012-821X(91)90218-7.

767 van Hinsbergen, D.J.J. et al., 2021, A record of plume-induced plate rotation triggering subduction
768 initiation: *Nature Geoscience*, v. 14, p. 626–630, doi:10.1038/s41561-021-00780-7.

769 van Hinsbergen, D.J.J., Steinberger, B., Doubrovine, P. V., and Gassmöller, R., 2011, Acceleration and
770 deceleration of India-Asia convergence since the Cretaceous: Roles of mantle plumes and continental
771 collision: *Journal of Geophysical Research: Solid Earth*, v. 116, p. 6101, doi:10.1029/2010JB008051.

772 Hofstetter, R., and Beyth, M., 2003, The afar depression: Interpretation of the 1960-2000 earthquakes:
773 *Geophysical Journal International*, v. 155, p. 715–732, doi:10.1046/j.1365-246X.2003.02080.x.

774 Hughes, G.W., Varol, O., and Beydoun, Z.R., 1991, Evidence for Middle Oligocene rifting of the Gulf of Aden
775 and for Late Oligocene rifting of the southern Red Sea: *Marine and Petroleum Geology*, v. 8, p. 354–
776 358, doi:10.1016/0264-8172(91)90088-l.

777 Huismans, R.S., Podladchikov, Y.Y., and Cloetingh, S., 2001, Transition from passive to active rifting:
778 Relative importance of asthenospheric doming and passive extension of the lithosphere: *Journal of*
779 *Geophysical Research: Solid Earth*, v. 106, p. 11271–11291, doi:10.1029/2000JB900424.

780 Ilani, S., Harlavan, Y., Tarawneh, K., Rabba, I., Weinberger, R., Ibrahim, K., Peltz, S., and Steinitz, G., 2001,
781 New K-Ar ages of basalts from the Harrat Ash Shaam volcanic field in Jordan: Implications for the
782 span and duration of the upper-mantle upwelling beneath the western Arabian plate: *Geology*, v. 29,
783 p. 171–174, doi:10.1130/0091-7613(2001)029<0171:NKAAOB>2.0.CO;2.

784 Ince, E.S., Barthelmes, F., Reißland, S., Elger, K., Förste, C., Flechtner, F., and Schuh, H., 2019, ICGEM – 15
785 years of successful collection and distribution of global gravitational models, associated services, and
786 future plans: *Earth System Science Data*, v. 11, p. 647–674, doi:10.5194/essd-11-647-2019.

787 Issachar, R., Ebbing, J., and Dilixiati, Y., 2022, New magnetic anomaly map for the Red Sea reveals
788 transtensional structures associated with rotational rifting: *Scientific Reports*, v. 12, p. 1–13,
789 doi:10.1038/s41598-022-09770-0.

790 Ivanov, A. V., Demonterova, E.I., He, H., Perepelov, A.B., Travin, A. V., and Lebedev, V.A., 2015, Volcanism
791 in the Baikal rift: 40years of active-versus-passive model discussion: *Earth-Science Reviews*, v. 148,
792 p. 18–43, doi:10.1016/j.earscirev.2015.05.011.

793 Joffe, S., and Garfunkel, Z., 1987, Plate kinematics of the Red Sea – a re-evaluation: *Tectonophysics*, v. 141,
794 p. 5–22.

795 Jolivet, L., and Faccenna, C., 2000, Mediterranean extension and the Africa-Eurasia collision: *Tectonics*, v.
796 19, p. 1095–1106, doi:10.1029/2000TC900018.

797 Keen, C.E., 1985, The dynamics of rifting: deformation of the lithosphere by active and passive driving
798 forces: *Geophys. J. R. ash. Soc*, v. 80, p. 95–120,
799 <https://academic.oup.com/gji/article/80/1/95/610547> (accessed August 2021).

800 Keir, D., Bastow, I.D., Pagli, C., and Chambers, E.L., 2013, The development of extension and magmatism
801 in the Red Sea rift of Afar: *Tectonophysics*, v. 607, p. 98–114, doi:10.1016/j.tecto.2012.10.015.

802 Keir, D., Pagli, C., Bastow, I.D., and Ayele, A., 2011, The magma-assisted removal of Arabia in Afar: Evidence
803 from dike injection in the Ethiopian rift captured using InSAR and seismicity: *Tectonics*, v. 30,
804 doi:<https://doi.org/10.1029/2010TC002785>.

805 Keranen, K., and Klemperer, S.L., 2008, Discontinuous and diachronous evolution of the Main Ethiopian
806 Rift : Implications for development of continental rifts: *Earth and Planetary Science Letters*, v. 265, p.
807 96–111, doi:10.1016/j.epsl.2007.09.038.

808 Kidane, T., 2016, Strong clockwise block rotation of the Ali-Sabieh/Aisha Block: Evidence for opening of the
809 Afar Depression by a “saloon-door” mechanism, *in* Geological Society Special Publication, Geological
810 Society of London, v. 420, p. 209–219, doi:10.1144/SP420.10.

811 Koppers, A.A.P., Becker, T.W., Jackson, M.G., Konrad, K., Müller, R.D., Romanowicz, B., Steinberger, B., and
812 Whittaker, J.M., 2021, Mantle plumes and their role in Earth processes: *Nature Reviews Earth &*
813 *Environment*, v. 2, p. 382–401, doi:10.1038/s43017-021-00168-6.

814 Koptev, A., Gerya, T., Calais, E., Leroy, S., and Burov, E., 2018, Afar triple junction triggered by plume-
815 assisted bi-directional continental break-up: *Scientific Reports*, v. 8, p. 1–7, doi:10.1038/s41598-018-
816 33117-3.

817 Leroy, S. et al., 2013, From rifting to oceanic spreading in the Gulf of Aden: A synthesis: *Frontiers in Earth*
818 *Sciences*, v. 5, p. 385–427, doi:10.1007/978-3-642-30609-9_20.

819 Lithgow-Bertelloni, C., and Silver, P.G., 1998, Dynamic topography, plate driving forces and the African
820 superswell: *Nature*, v. 395, p. 269–272, doi:10.1038/26212.

821 Macdonald, K., Sempere, J.C., and Fox, P.J., 1984, East Pacific Rise from Siqueiros to Orozco fracture zones:
822 along- strike continuity of axial neovolcanic zone and structure and evolution of overlapping
823 spreading centers.: *Journal of Geophysical Research*, v. 89, p. 6049–6069,
824 doi:10.1029/JB089iB07p06049.

825 Maestrelli, D., Brune, S., Corti, G., Keir, D., Muluneh, A.A., and Sani, F., 2022, Analog and Numerical
826 Modeling of Rift-Rift-Rift Triple Junctions: *Tectonics*, v. 41, p. e2022TC007491,
827 doi:<https://doi.org/10.1029/2022TC007491>.

828 Manighetti, I., Tapponnier, P., Courtillot, V., Gallet, Y., Jacques, E., and Gillot, P.Y., 2001, Strain transfer
829 between disconnected, propagating rifts in Afar: *Journal of Geophysical Research: Solid Earth*, v. 106,
830 p. 13613–13665, doi:10.1029/2000jb900454.

831 Mattash, M.A., Pinarelli, L., Vaselli, O., Minissale, A., Al-Kadasi, M., Shawki, M.N., and Tassi, F., 2013,
832 Continental Flood Basalts and Rifting: Geochemistry of Cenozoic Yemen Volcanic Province:
833 *International Journal of Geosciences*, v. 04, p. 1459–1466, doi:10.4236/ijg.2013.410143.

834 McConnell, R., and Baker, B., 1970, The Structural Pattern of the Afro-Arabian Rift System in Relation to
835 Plate Tectonics: Discussion: *Philosophical Transactions of the Royal Society of London Series A*, v.
836 267, p. 390–391, https://www.jstor.org/stable/73628?seq=3#metadata_info_tab_contents
837 (accessed August 2021).

838 McDougall, I. an, and Brown, F.H., 2009, Timing of volcanism and evolution of the northern Kenya Rift:
839 *Geological Magazine*, v. 146, p. 34–47, doi:DOI: 10.1017/S0016756808005347.

840 Meshesha, D., and Shinjo, R., 2008, Rethinking geochemical feature of the Afar and Kenya mantle plumes
841 and geodynamics implications: *Journal of Geophysical Research: Solid Earth*, v. 113, p. 9209,

842 doi:10.1029/2007JB005549.

843 Mitchell, N.C., and Bosworth, (in press), W. The tectonic stability of Arabia, *in* Rasul, N.M.A. and Stewart,
844 I.C.F. eds., The tectonic stability of Arabia, in *Rifting and sediments in the Red Sea and Arabian Gulf*
845 regions, Taylor & Francis.

846 Mitchell, N.C., and Sofianos, S.S., 2018, Origin of submarine channel north of hanish sill, red sea, *in*
847 Geological Setting, Palaeoenvironment and Archaeology of the Red Sea, Springer International
848 Publishing, p. 259–273, doi:10.1007/978-3-319-99408-6_12.

849 Mitra, S., Mitra, K., Gupta, S., Bhattacharya, S., Chauhan, P., and Jain, N., 2017, Alteration and submergence
850 of basalts in Kachchh, Gujarat, India: implications for the role of the Deccan Traps in the India–
851 Seychelles break-up: Geological Society, London, Special Publications, v. 445, p. 47–67,
852 doi:10.1144/SP445.9.

853 Morag, N., Haviv, I., Eyal, M., Kohn, B.P., and Feinstein, S., 2019, Early flank uplift along the Suez Rift:
854 Implications for the role of mantle plumes and the onset of the Dead Sea Transform: *Earth and*
855 *Planetary Science Letters*, v. 516, p. 56–65, doi:10.1016/j.epsl.2019.03.002.

856 Moretti, I., and Froidevaux, C., 1986, Thermomechanical models of active rifting: *Tectonics*, v. 5, p. 501–
857 511, doi:10.1029/TC005I004P00501.

858 Morgan, W.J., 1971, Convection plumes in the lower mantle: *Nature*, v. 230, p. 42–43,
859 doi:10.1038/230042a0.

860 Okwokwo, O.I., Mitchell, N.C., Shi, W., Stewart, I.C.F., and Izzeldin, A.Y., 2022, How have thick evaporites
861 affected early seafloor spreading magnetic anomalies in the Central Red Sea? *Geophysical Journal*
862 *International*, v. 229, p. 1550–1566, doi:10.1093/gji/ggac012.

863 Pagli, C., Wang, H., Wright, T.J., Calais, E., and Lewi, E., 2014, Current plate boundary deformation of the
864 Afar rift from a 3-D velocity field inversion of InSAR and GPS: *Journal of Geophysical Research: Solid*
865 *Earth*, v. 119, p. 8562–8575, doi:https://doi.org/10.1002/2014JB011391.

866 Pagli, C., Yun, S.-H., Ebinger, C., Keir, D., and Wang, H., 2018, Strike-slip tectonics during rift linkage:
867 *Geology*, v. 47, p. 31–34, doi:10.1130/G45345.1.

868 Peate, I.U., Baker, J.A., Al-Kadasi, M., Al-Subbary, A., Knight, K.B., Riisager, P., Thirlwall, M.F., Peate, D.W.,
869 Renne, P.R., and Menzies, M.A., 2005, Volcanic stratigraphy of large-volume silicic pyroclastic
870 eruptions during Oligocene Afro-Arabian flood volcanism in Yemen: *Bulletin of Volcanology*, v. 68, p.
871 135–156, doi:10.1007/s00445-005-0428-4.

872 Le Pichon, X., and Gaulier, J.-M., 1988, The rotation of Arabia and the Levant fault system: *Tectonophysics*,
873 v. 153, p. 271–294, doi:10.1016/0040-1951(88)90020-0.

874 Plaziat, J.-C., Baltzer, F., Choukri, A., Conchon, O., Freytet, P., Orszag-Sperber, F., Raguideau, A., and Reyss,
875 J.-L., 1998, Quaternary marine and continental sedimentation in the northern Red Sea and Gulf of
876 Suez (Egyptian coast): influences of rift tectonics, climatic changes and sea-level fluctuations, *in*
877 *Sedimentation and Tectonics in Rift Basins Red Sea:- Gulf of Aden*, Springer Netherlands, p. 537–573,
878 doi:10.1007/978-94-011-4930-3_29.

879 Prave, A.R., Bates, C.R., Donaldson, C.H., Toland, H., Condon, D.J., Mark, D., and Raub, T.D., 2016, Geology
880 and geochronology of the Tana Basin, Ethiopia: LIP volcanism, Super eruptions and Eocene-Oligocene
881 environmental change: *Earth and Planetary Science Letters*, v. 443, p. 1–8,
882 doi:10.1016/j.epsl.2016.03.009.

883 Pusok, A.E., and Stegman, D.R., 2020, The convergence history of India-Eurasia records multiple

884 subduction dynamics processes: *Science Advances*, v. 6,
885 doi:10.1126/SCIADV.AAZ8681/SUPPL_FILE/AAZ8681_SM.PDF.

886 Qaysi, S., Liu, K.H., and Gao, S.S., 2018, A Database of Shear-Wave Splitting Measurements for the Arabian
887 Plate: *Seismological Research Letters*, v. 89, p. 2294–2298, doi:10.1785/0220180144.

888 Reilinger, R. et al., 2006, GPS constraints on continental deformation in the Africa-Arabia-Eurasia
889 continental collision zone and implications for the dynamics of plate interactions: *Journal of*
890 *Geophysical Research-Solid Earth*, v. 111.

891 Reilinger, R., and McClusky, S., 2011, Nubia-Arabia-Eurasia plate motions and the dynamics of
892 Mediterranean and Middle East tectonics: *Geophysical Journal International*, v. 186, p. 971–979,
893 doi:10.1111/j.1365-246X.2011.05133.x.

894 Richards, M.A., Duncan, R.A., and Courtillot, V.E., 1989, Flood basalts and hot-spot tracks: Plume heads
895 and tails: *Science*, v. 246, p. 103–107, doi:10.1126/science.246.4926.103.

896 Rime, V., Foubert, A., Ruch, J., and Kidane, T., 2023, Tectonostratigraphic evolution and significance of the
897 Afar Depression: *Earth-Science Reviews*, v. 244, p. 104519,
898 doi:https://doi.org/10.1016/j.earscirev.2023.104519.

899 Roger, J., Platel, J.P., Cavelier, C., and Bourdillon-de-Grissac, C., 1989, Données nouvelles sur la
900 stratigraphie et l’histoire géologique du Dhofar (Sultanat d’Oman): *Bulletin de la Société géologique*
901 *de France*, v. 2, p. 256–277, In France, abstract in English.

902 Rooney, T.O., 2017, The Cenozoic magmatism of East-Africa: Part I — Flood basalts and pulsed magmatism:
903 *Lithos*, v. 286–287, p. 264–301, doi:10.1016/j.lithos.2017.05.014.

904 Sandwell, D.T., Müller, R.D., Smith, W.H.F., Garcia, E., and Francis, R., 2014, New global marine gravity
905 model from CryoSat-2 and Jason-1 reveals buried tectonic structure: *Science*, v. 346, p. 65–67,
906 doi:10.1126/SCIENCE.1258213.

907 Schettino, A., Macchiavelli, C., Pierantoni, P.P., Zanoni, D., and Rasul, N., 2016, Recent kinematics of the
908 tectonic plates surrounding the red sea and gulf of aden: *Geophysical Journal International*, v. 207,
909 p. 457–480, doi:10.1093/gji/ggw280.

910 Schettino, A., Macchiavelli, C., and Rasul, N.M.A., 2018, Plate motions around the red sea since the early
911 oligocene, *in Geological Setting, Palaeoenvironment and Archaeology of the Red Sea*, Springer
912 International Publishing, p. 203–220, doi:10.1007/978-3-319-99408-6_9.

913 Schult, A., 1974, Palaeomagnetism of tertiary volcanic rocks from the Ethiopian southern plateau and the
914 Danakil block: *Journal of Geophysics*, v. 40, p. 203–212,
915 <https://journal.geophysicsjournal.com/JofG/article/view/277> (accessed June 2021).

916 Sembroni, A., Faccenna, C., Becker, T.W., Molin, P., and Abebe, B., 2016, Long-term, deep-mantle support
917 of the Ethiopia-Yemen Plateau: *Tectonics*, v. 35, p. 469–488, doi:10.1002/2015TC004000.Received.

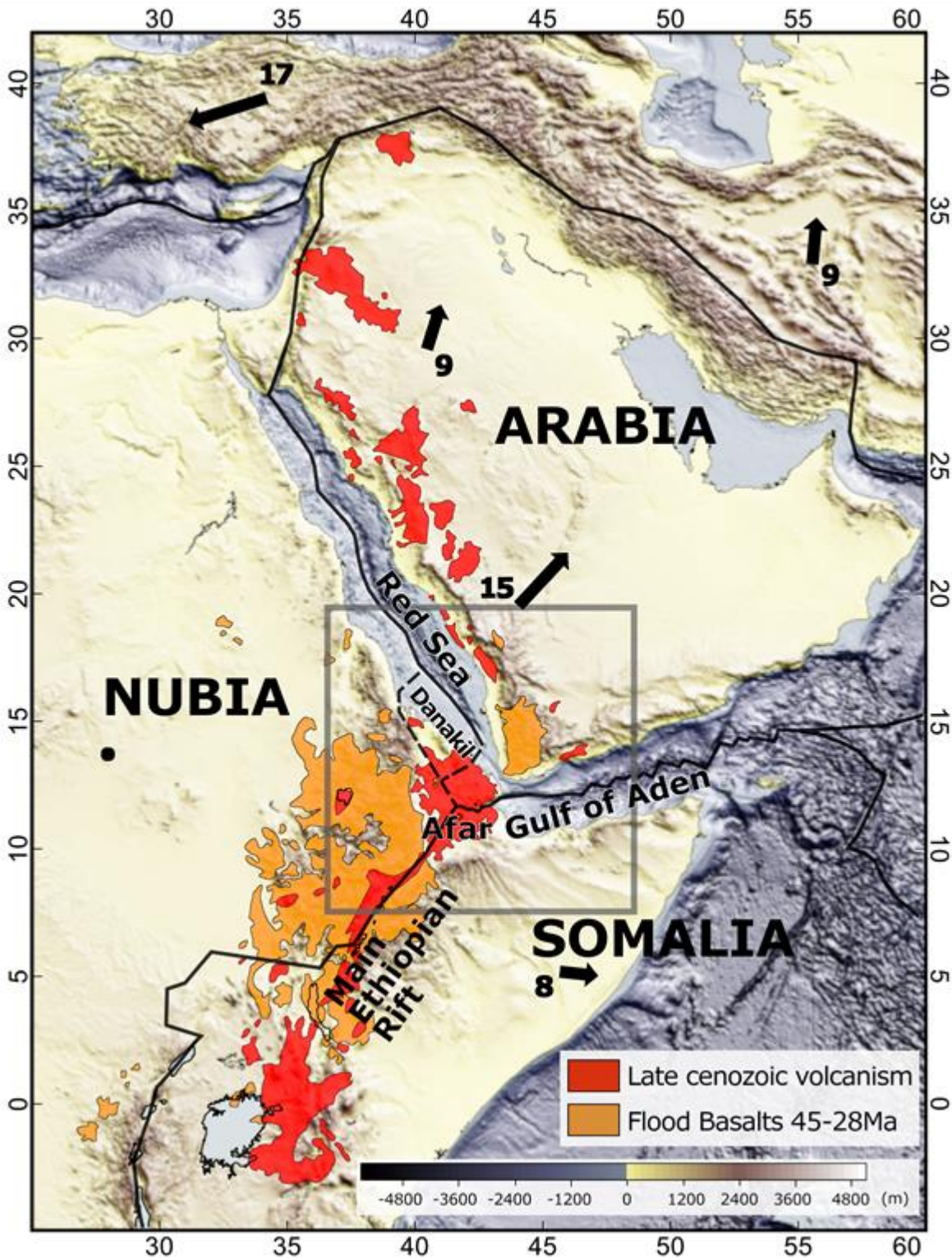
918 Sengör, A.M.C., and Burke, K., 1978, Relative timing of rifting and volcanism on Earth and its tectonic
919 implications: *Geophysical Research Letters*, v. 5, p. 419–421, doi:10.1029/GL005I006P00419.

920 Sobolev, S. V., Sobolev, A. V., Kuzmin, D. V., Krivolutskaya, N.A., Petrunin, A.G., Arndt, N.T., Radko, V.A.,
921 and Vasiliev, Y.R., 2011, Linking mantle plumes, large igneous provinces and environmental
922 catastrophes: *Nature*, v. 477, p. 312–316, doi:10.1038/nature10385.

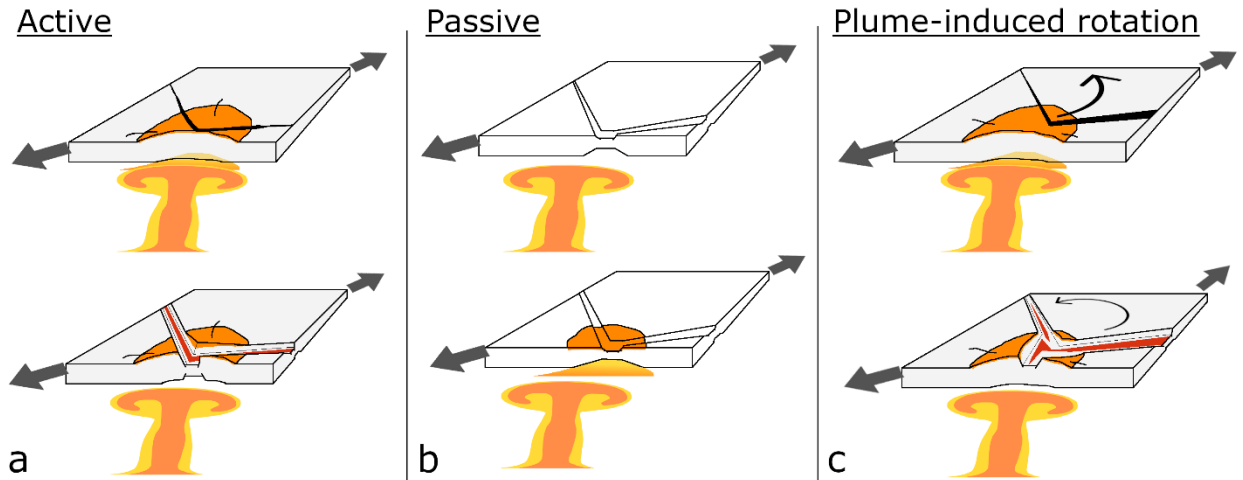
923 Stamps, D.S., Flesch, L.M., Calais, E., and Ghosh, A., 2014, Current kinematics and dynamics of Africa and
924 the East African Rift System: *Journal of Geophysical Research: Solid Earth*, v. 119, p. 5161–5186,
925 doi:10.1002/2013JB010717.

- 926 Stockli, D.F., and Bosworth, W.B., 2018, Timing of extensional faulting along the magma-poor central and
 927 northern red sea rift margin-transition from regional extension to necking along a hyperextended
 928 rifted margin, *in* Geological Setting, Palaeoenvironment and Archaeology of the Red Sea, Springer
 929 International Publishing, p. 81–111, doi:10.1007/978-3-319-99408-6_5.
- 930 Su, H., and Zhou, J., 2020, Timing of Arabia-Eurasia collision: Constraints from restoration of crustal-scale
 931 cross-sections: *Journal of Structural Geology*, v. 135, p. 104041, doi:10.1016/j.jsg.2020.104041.
- 932 Szymanski, E., Stockli, D.F., Johnson, P.R., and Hager, C., 2016, Thermochronometric evidence for diffuse
 933 extension and two-phase rifting within the Central Arabian Margin of the Red Sea Rift: *Tectonics*, v.
 934 35, p. 2863–2895, doi:10.1002/2016TC004336.
- 935 Tazieff, H.T., Varet, J., Barberi, F., and Giglia, G., 1972, Tectonic significance of the Afar (or Danakil)
 936 depression: *Nature*, v. 235, p. 144–147.
- 937 Tesfaye, S., Harding, D.J., and Kusky, T.M., 2003, Early continental breakup boundary and migration of the
 938 Afar triple junction, Ethiopia: *Bulletin of the Geological Society of America*, v. 115, p. 1053–1067,
 939 doi:10.1130/B25149.1.
- 940 Varet, J., 2018, *Geology of Afar (East Africa)*: 1–249 p.
- 941 Varet, J., 1978, *Geology of central and southern Afar (Ethiopia and Djibouti Republic)*: Paris, Centre
 942 national de la recherche scientifique.
- 943 Viltres, R., Jónsson, S., Alothman, A.O., Liu, S., Leroy, S., Masson, F., Doubre, C., and Reilinger, R., 2022,
 944 Present-Day Motion of the Arabian Plate: *Tectonics*, v. 41, p. e2021TC007013,
 945 doi:https://doi.org/10.1029/2021TC007013.
- 946 Viltres, R., Jónsson, S., Ruch, J., Doubre, C., Reilinger, R., Floyd, M., and Ogubazghi, G., 2020, Kinematics
 947 and deformation of the southern Red Sea region from GPS observations: *Geophysical Journal
 948 International*, v. 221, p. 2143–2154, doi:10.1093/gji/ggaa109.
- 949 Watchorn, F., Nichols, G.J., and Bosence, D.W.J., 1998, Rift-related sedimentation and stratigraphy,
 950 southern Yemen (Gulf of Aden), *in* Sedimentation and Tectonics in Rift Basins Red Sea:- Gulf of Aden,
 951 Springer Netherlands, p. 165–189, doi:10.1007/978-94-011-4930-3_11.
- 952 Wescott, W.A., Wigger, S.T., Stone, D.M., and Morley, C.K., 1999, *AAPG Studies in Geology# 44, Chapter 3:*
 953 *Geology and Geophysics of the Lotikipi Plain*:
- 954 White, R., and McKenzie, D., 1989, Magmatism at rift zones: the generation of volcanic continental margins
 955 and flood basalts: *Journal of Geophysical Research*, v. 94, p. 7685–7729,
 956 doi:10.1029/JB094iB06p07685.
- 957 White, R.S., and McKenzie, D., 1995, Mantle plumes and flood basalts: *Journal of Geophysical Research*, v.
 958 100, p. 543–560, doi:10.1029/95jb01585.
- 959 Will, T.M., and Frimmel, H.E., 2018, Where does a continent prefer to break up? Some lessons from the
 960 South Atlantic margins: *Gondwana Research*, v. 53, p. 9–19, doi:10.1016/j.gr.2017.04.014.
- 961 Wilson, J.T., 1963, A possible origin of the Hawaiian Islands: *Canadian Journal of Physics*, v. 41, p. 863–870,
 962 doi:10.1139/P63-094.
- 963 Wolfenden, E., Ebinger, C., Yirgu, G., Deino, A., and Ayalew, D., 2004, Evolution of the northern Main
 964 Ethiopian rift: Birth of a triple junction: *Earth and Planetary Science Letters*, v. 224, p. 213–228,
 965 doi:10.1016/j.epsl.2004.04.022.
- 966 Zingerle, P., Pail, R., Gruber, T., and Oikonomidou, X., 2020, The combined global gravity field model

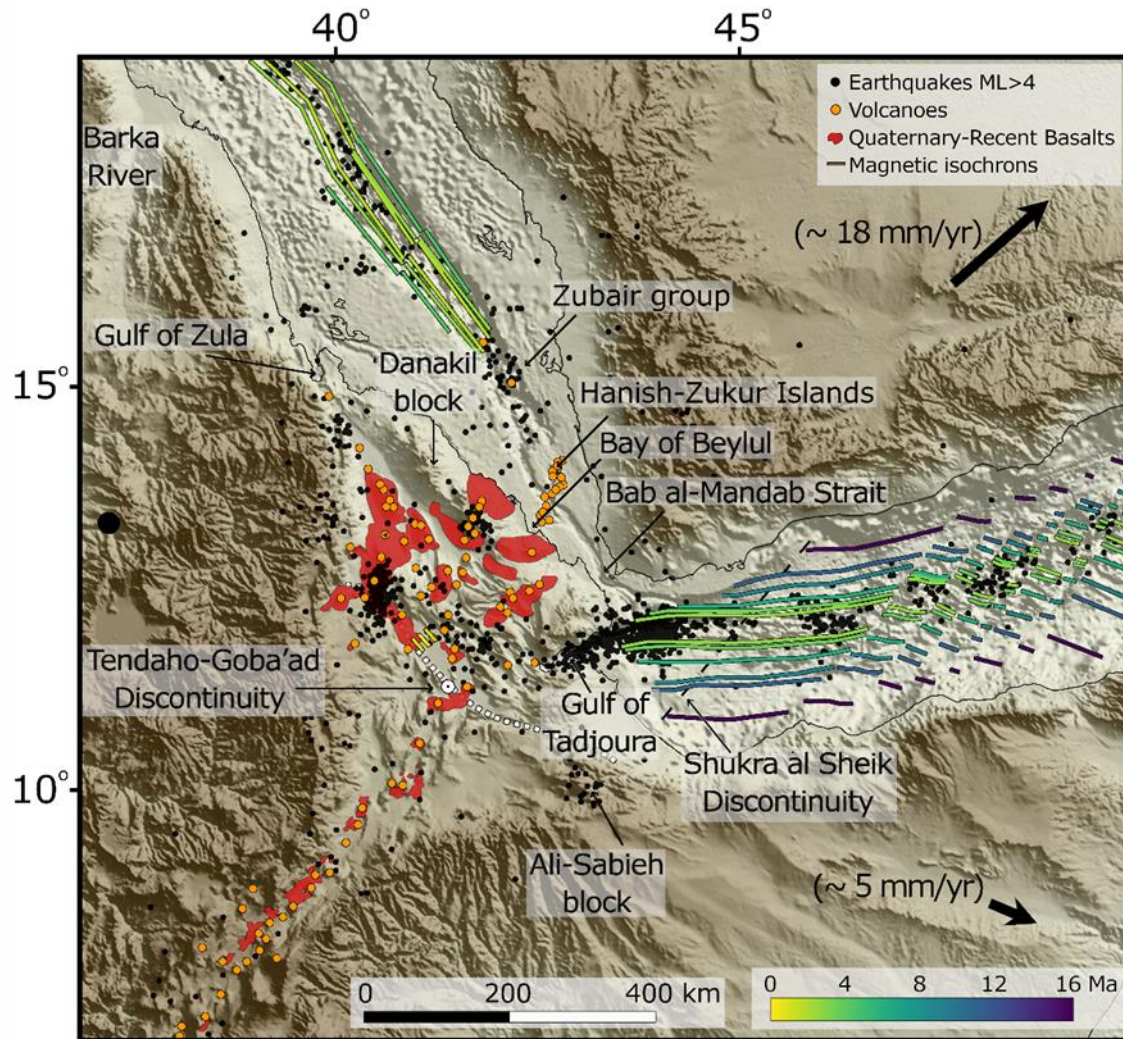
967 XGM2019e: Journal of Geodesy 2020 94:7, v. 94, p. 1–12, doi:10.1007/S00190-020-01398-0.
968 Zwaan, F., Corti, G., Keir, D., and Sani, F., 2020a, A review of tectonic models for the rifted margin of Afar:
969 Implications for continental break-up and passive margin formation: Journal of African Earth
970 Sciences, v. 164, doi:10.1016/j.jafrearsci.2019.103649.
971 Zwaan, F., Corti, G., Sani, F., Keir, D., Muluneh, A.A., Illsley-Kemp, F., and Papini, M., 2020b, Structural
972 Analysis of the Western Afar Margin, East Africa: Evidence for Multiphase Rotational Rifting:
973 Tectonics, v. 39, doi:10.1029/2019TC006043.
974
975



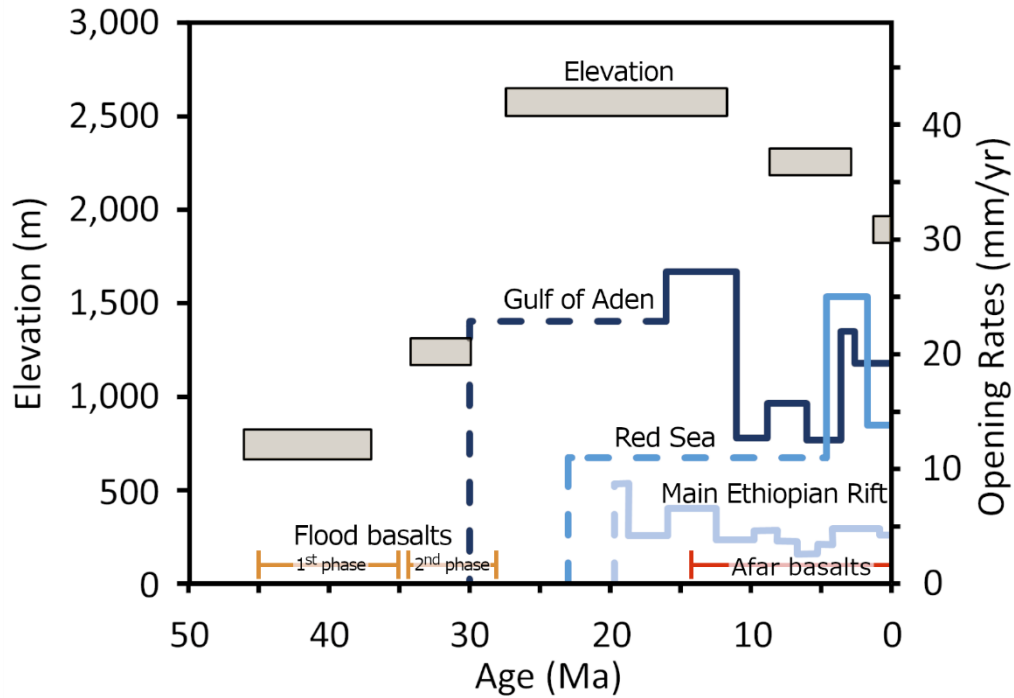
976
 977 **Figure 1.** Elevation map of the study area, showing the general plate tectonic configuration (from USGS
 978 and from Viltres et al. (2020) in the Afar region) and Cenozoic volcanics (modified from Varet, 1978;
 979 Davison et al., 1994; Beyene and Abdelsalam, 2005; Bosworth and Stockli, 2016) Black arrows indicate GPS
 980 velocities in respect to Nubia (modified from Reilinger et al., 2006).



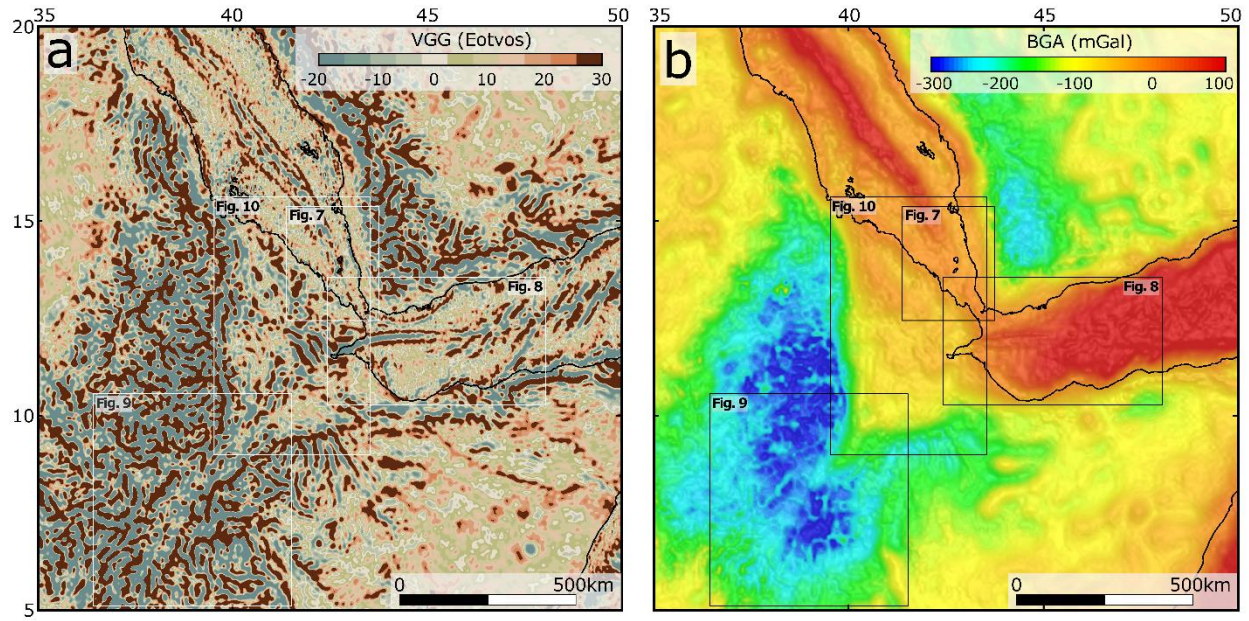
981
 982 **Figure 2.** Schematic mechanisms for plume-rift association in the Afro-Arabian rift. (a) Active mechanism,
 983 in which rifting results from the actively rising head of the Afar plume. In this mechanism impinging and
 984 eroding the base of the lithosphere prompt uplift and decompression melting and flood basalts volcanism.
 985 These introduce internal extensional forces and ultimately lead to break-up. (b) Passive mechanism, in
 986 which rifting is initiated solely by the remote stresses, regardless of underlying Afar plume. In this
 987 mechanism the production of massive volcanism is allowed when the thinned and stretched lithosphere
 988 is underlain by the thermal anomaly in the mantle. Flood basalts volcanism is generated by
 989 passively rising decompression melting of hot asthenospheric mantle. (c) Plume-induced plate rotation, in
 990 which lateral forces, induced by the arrival of the Afar plume head, add up to the remote stresses to change
 991 the plate kinematics. In this mechanism flood basalts volcanism is actively controlled, however, rifting is
 992 triggered by the new plate kinematics.



993
 994 **Figure 3.** Map of the Afar region showing magnetic isochrons (modified from Fournier et al., 2010; Bridges
 995 et al., 2012; Schettino et al., 2016), earthquake locations (from ISC catalog), Holocene onshore volcano
 996 locations (from GVP catalog and Viltres et al. (2020)) and recent volcanism (modified from Keir et al., 2013).



997
 998 **Figure 4.** Elevation of the Ethiopian–Yemen plateau (after Sembroni et al., 2016; Faccenna et al., 2019),
 999 volcanic episodes and opening rates of the rift arms (modified from Fournier et al., 2010; DeMets and
 1000 Merkouriev, 2016; Schettino et al., 2018). Dashed lines indicate estimations from geological observations
 1001 and solid lines from magnetic isochrons.

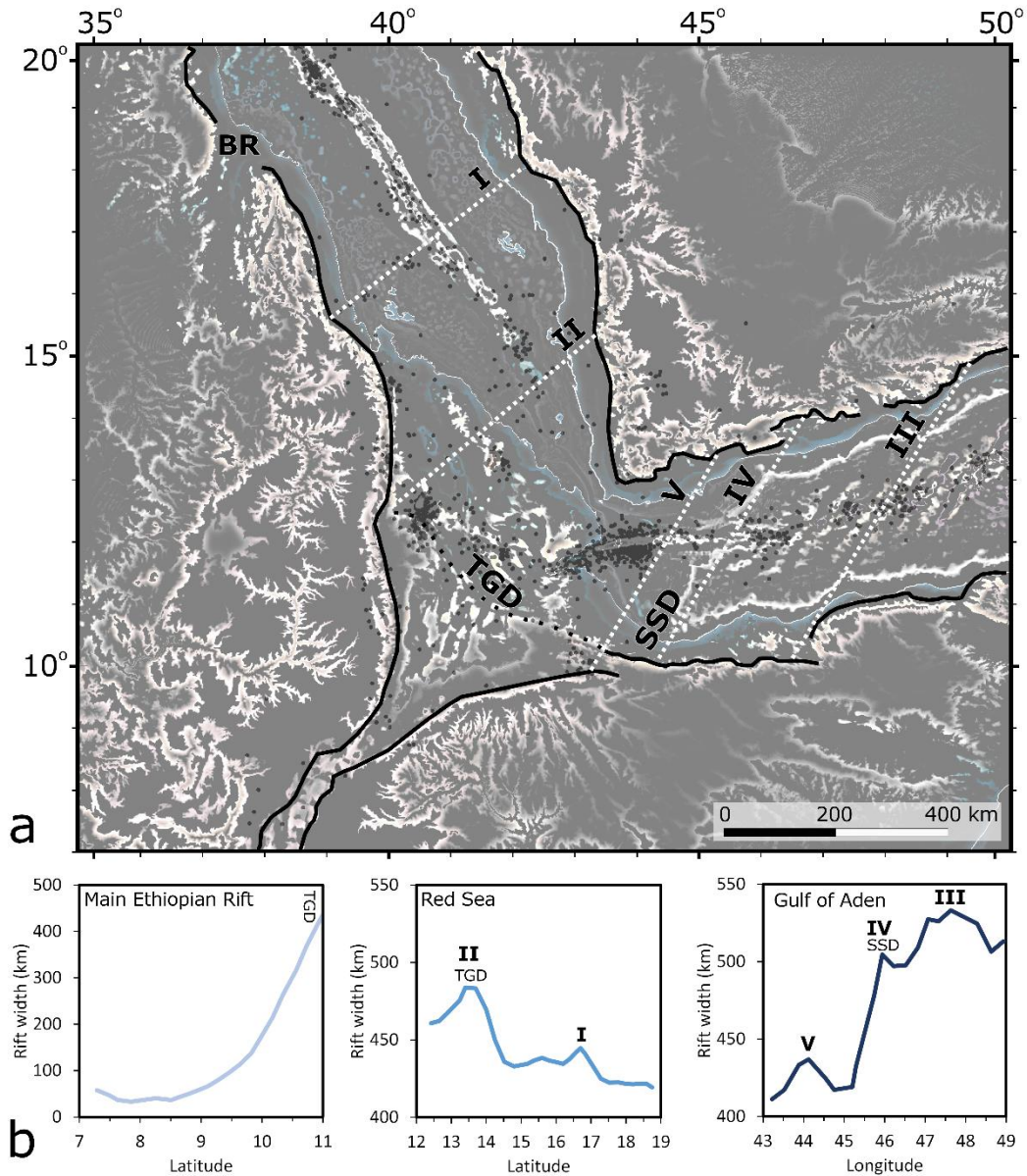


1007

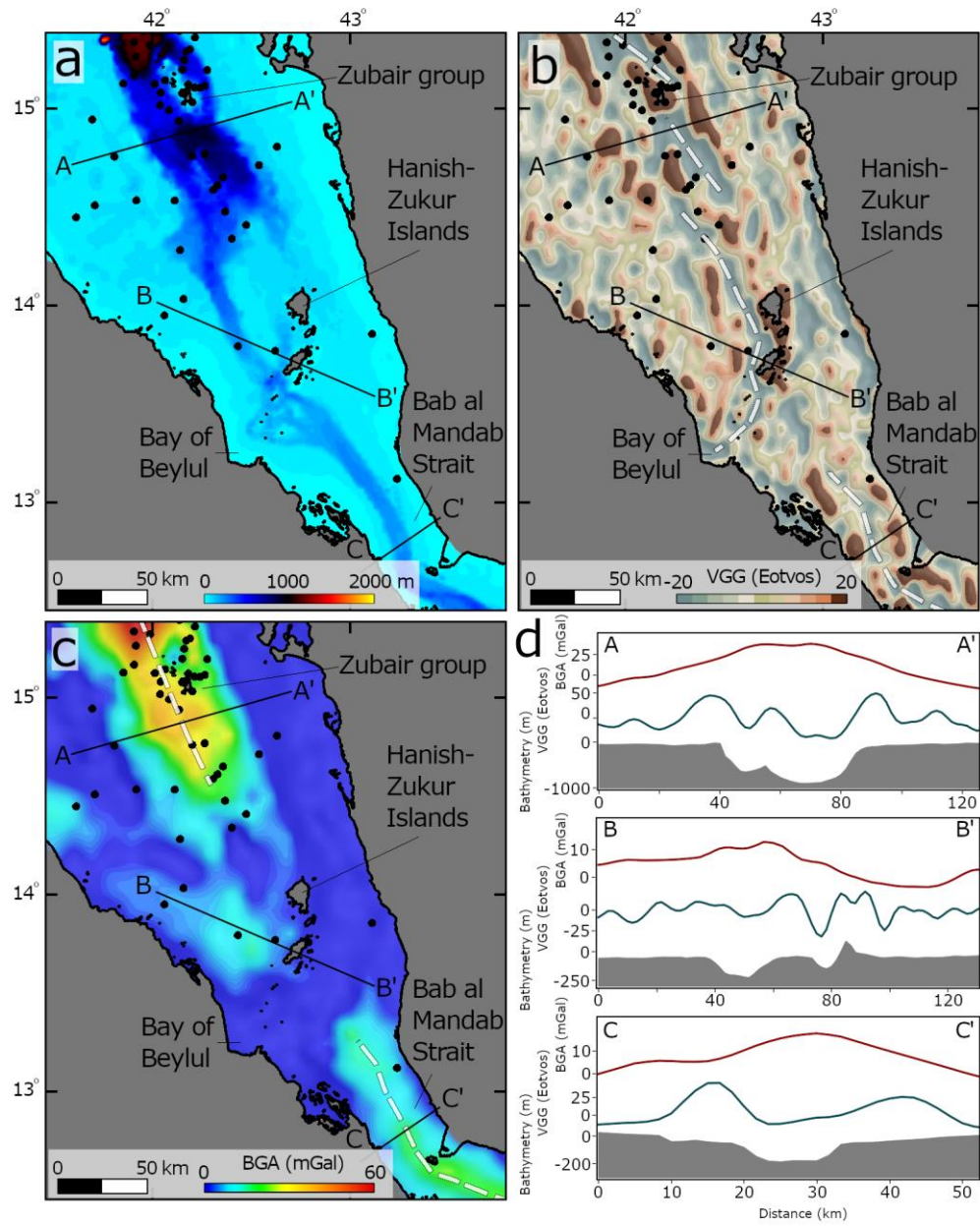
1008

1009

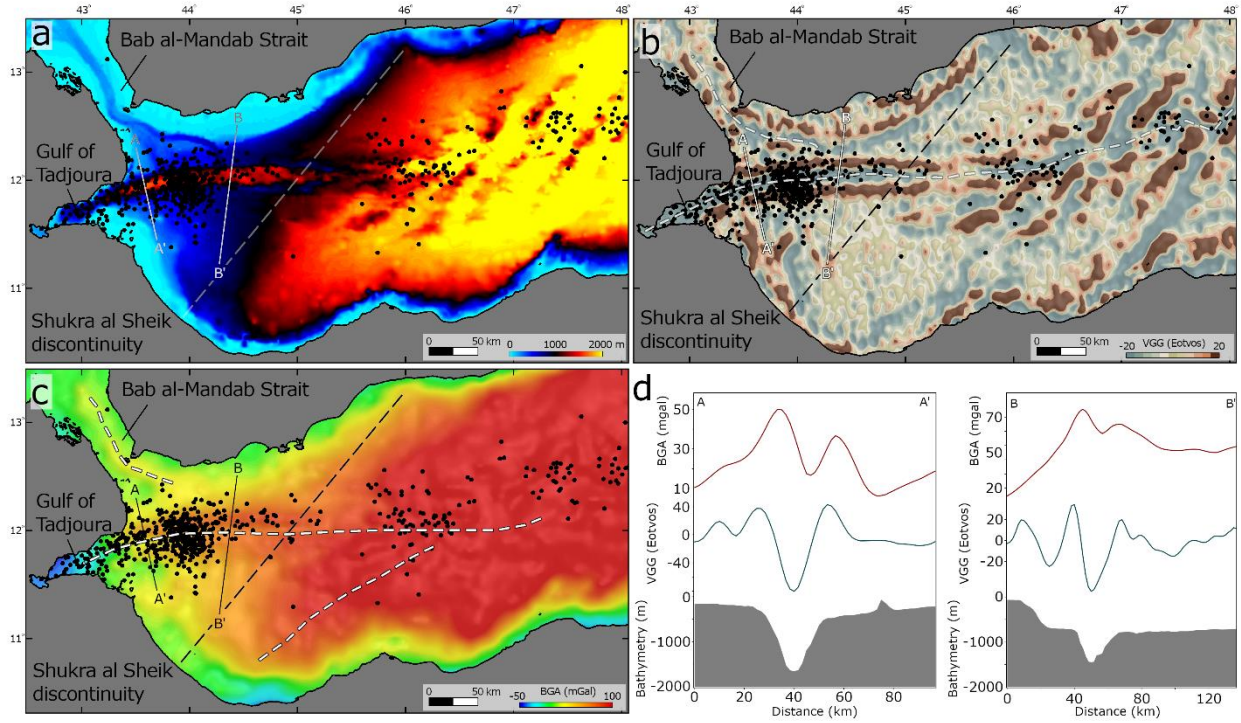
Figure 5. Gravity data of the Afar region. (a) Vertical gravity gradient from Sandwell et al. (2014). (b) Bouguer anomaly model from ICGEM, XGM2019e (Zingerle et al., 2020).



1010
 1011 **Figure 6.** (a) Difference of Gaussians applied to topography and bathymetry showing rift margins (black
 1012 lines). White dashed lines indicate peaks in rift width. TGD is the Tendaho-Goba'ad Discontinuity. SSD is
 1013 the Shukra al Sheik discontinuity. Black dots indicate earthquake locations (ISC catalog). (b) Rift widths,
 1014 calculated in rift-perpendicular directions.



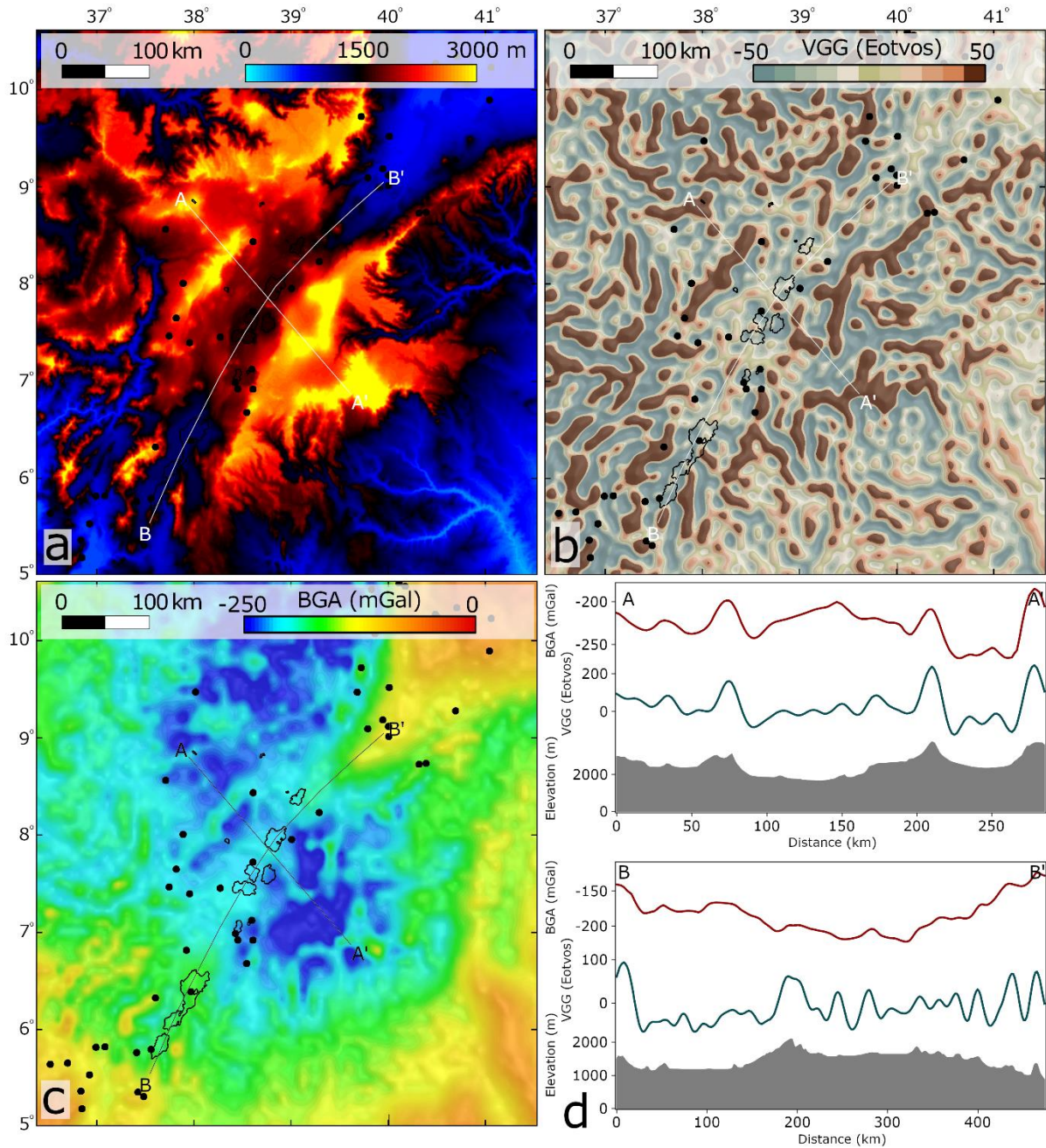
1015
 1016 **Figure 7.** Bathymetry (a), vertical gravity gradient (b) and Bouguer anomaly (c) in the southern Red Sea.
 1017 Black dots indicate earthquake locations (ISC catalog). (d) Profiles across rift axis.



1018

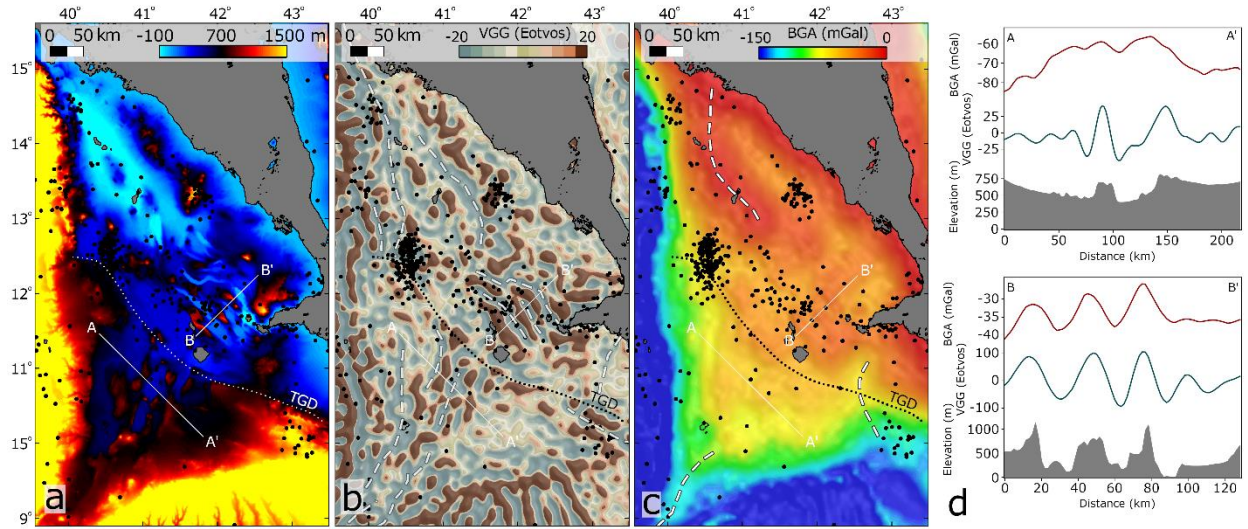
1019 **Figure 8.** Bathymetry (a), vertical gravity gradient (b) and Bouguer anomaly (c) in the Western Gulf of Aden.

1020 Black dots indicate earthquake locations (ISC catalog). (d) Profiles across rift axis.

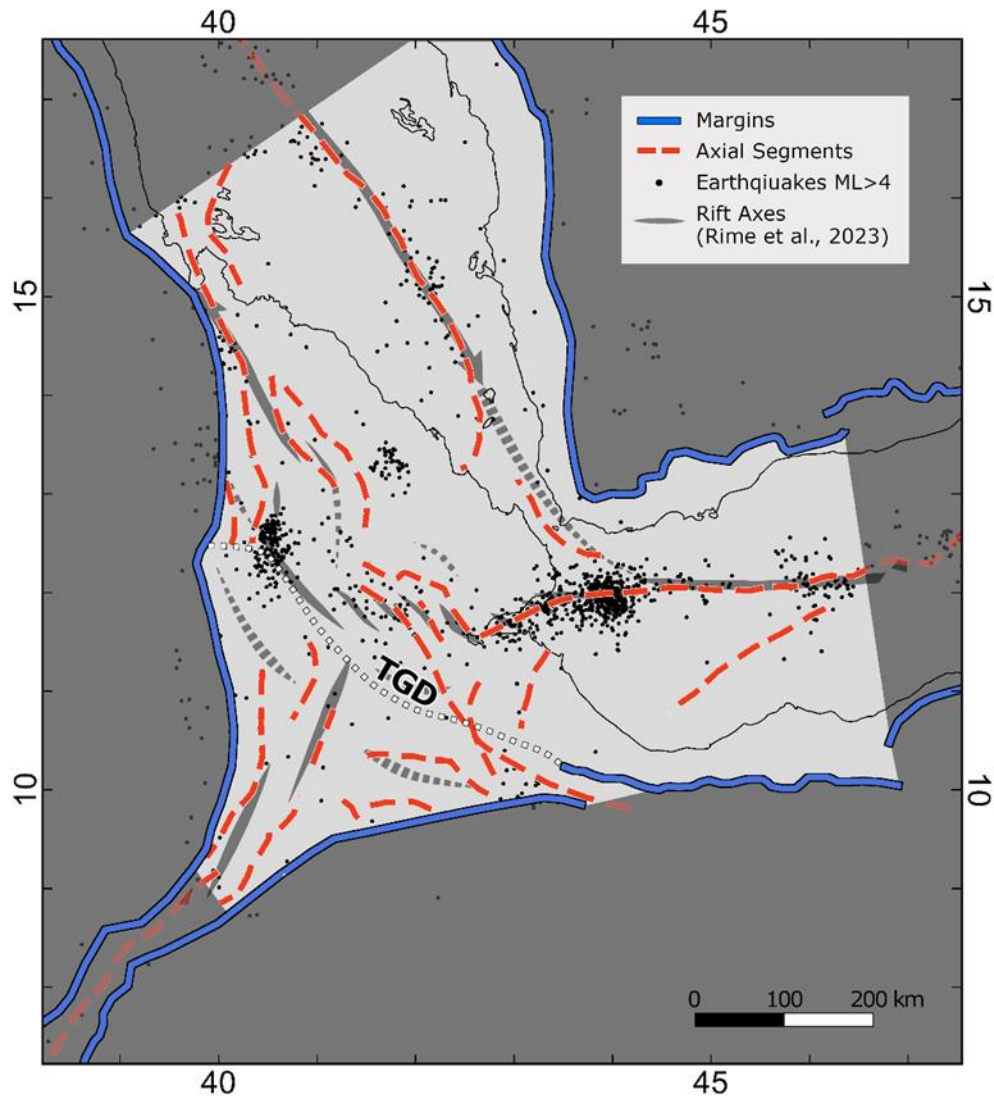


1021

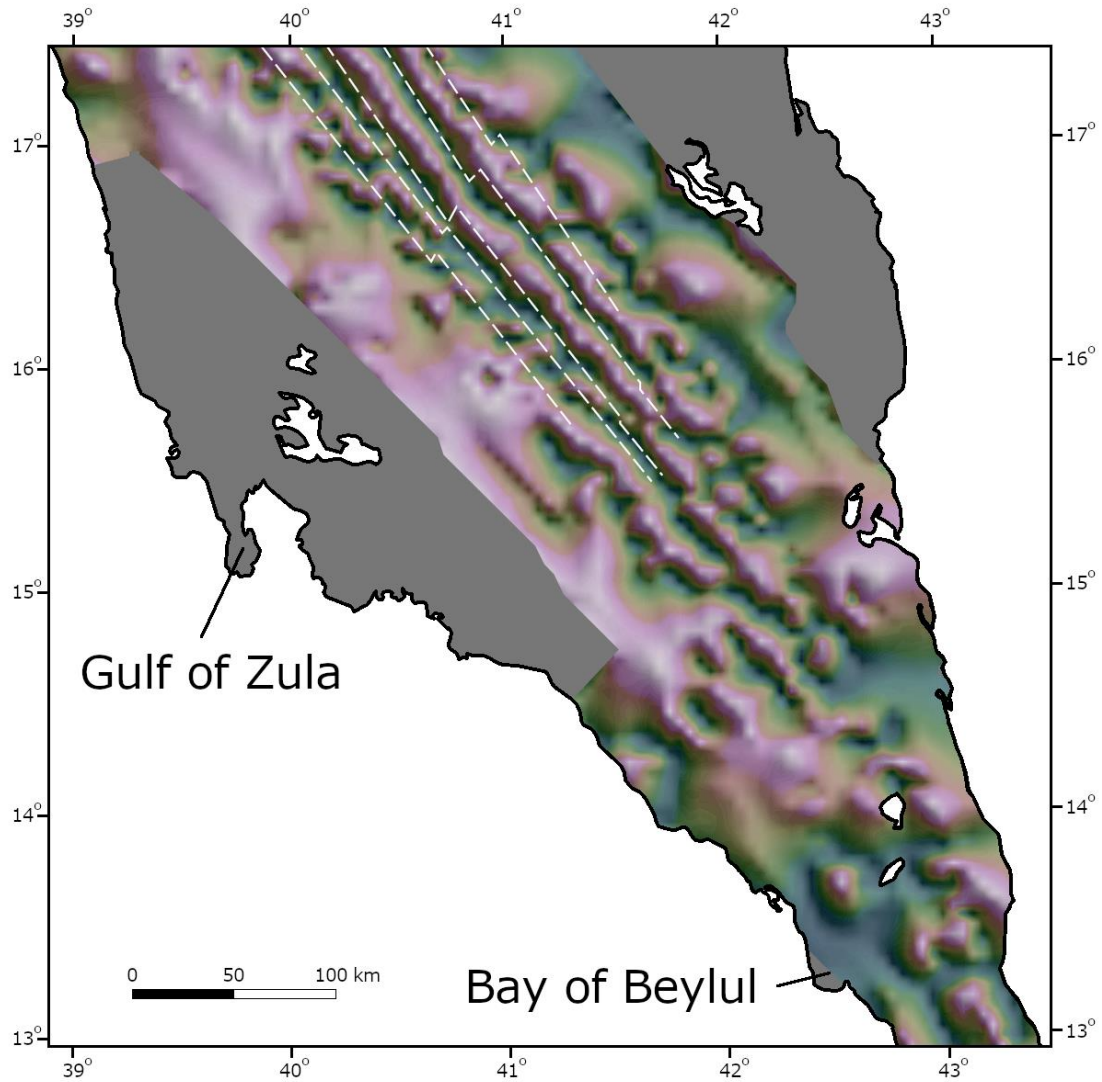
1022 **Figure 9.** Topography (a), vertical gravity gradient (b) and Bouguer anomaly (c) in the northern Main
 1023 Ethiopian Rift. Black dots indicate earthquake locations (ISC catalog). (d) Profiles across (AA') and along
 1024 (BB') the rift valley.



1025
 1026 **Figure 10.** Topography (a), vertical gravity gradient (b) and Bouguer anomaly (c) in the Afar triangle. Black
 1027 dots indicate earthquake locations (ISC catalog). TGD is the Tendaho-Goba'ad Discontinuity. (d) Profiles
 1028 SW (AA') and NE (BB') to the TGD.

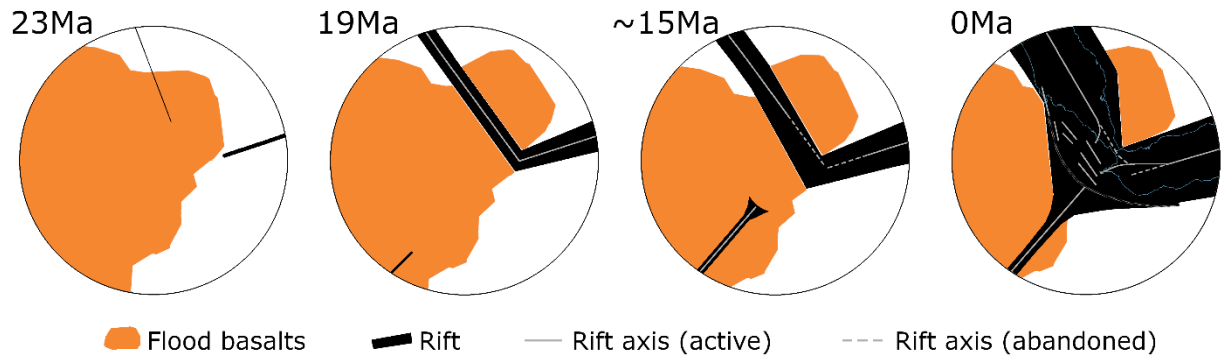


1029
 1030 **Figure 11.** Rift margins (solid white lines) and axial segments (long dashed black lines) in the Afar region.
 1031 Black dots indicate earthquake locations (ISC catalog). TGD is the Tendaho-Goba'ad Discontinuity. Rift axes
 1032 based on field observations after Rime et al. (2023).



1033
 1034 **Figure 12.** Tilt-angle derivative map of magnetic anomalies, projected on a shaded relief after Issachar et
 1035 al. (2022). Purple ~~colorseolures~~ represent positive angles and green colors represent negative angles.
 1036 White dashed lines indicate magnetic stripes (Schettino et al., 2016).

1037
 1038
 1039
 1040
 1041
 1042
 1043



1044

1045

Figure 13. Synthesis of the progressive development of the rift intersections.